The Equatorial Mesoscale Experiment (EMEX): An Overview

Peter J. Webster* and
Robert A. Houze, Jr.+

Abstract

During the Southern Hemisphere summer, an aircraft research program (EMEX: the Equatorial Monsoon Experiment) was conducted over the tropical ocean north of Australia to investigate the mesoscale convective systems in the monsoon flow. EMEX was conducted concurrently and in the same location as the Australian Monsoon Experiment (AMEX) and the Stratosphere–Troposphere Exchange Program (STEP). Airborne Doppler radar and other aircraft instrumentation were used to document the horizontal and vertical air motions in ten major cloud systems. The EMEX airborne platforms were supplemented by a surface Doppler radar and the enhanced AMEX upper-air sounding network. The data obtained should significantly enhance the knowledge of vertical motions in tropical clouds and thereby lead to a better understanding of how these clouds influence the large-scale tropical circulation and climate. An overview of the project is given in which the weather situations are reviewed and examples of the data are shown. Some initial results are discussed, together with their significance to the scientific objectives of EMEX and the parent program, the Tropical Ocean Global Atmosphere Program (TOGA).

1. Introduction

The Equatorial Mesoscale Experiment (EMEX) was conducted over the tropical oceanic area north of Australia in January–February 1987, during the Southern Hemisphere (austral) summer. The program explored the vertical air motions and other kinematic properties of tropical mesoscale convective-cloud systems ("cloud clusters") by direct aircraft penetration. The project was organized to coincide with two other major experimental programs being conducted in the region at the same time. The Australian Monsoon Experiment (AMEX) (see Holland et al. 1986) was a program of enhanced upper-air soundings and radar data collection in northern Australia, aimed at better documentation of those large-scale weather patterns over Australia that are associated with the ebb and flow of the Australian monsoon. AMEX provided an excellent synoptic context for the convective and mesoscale measurements obtained in EMEX. The Stratosphere–Troposphere Exchange Program (STEP) was conducted to obtain high-level aircraft measurements of trace chemicals, radiation, and other quantities above tropical convection in the region with the aim of understanding tropospheric–stratospheric interaction. These data added to those collected with the lower flying EMEX aircraft. The combination of these three independent but interlocking programs constituted a comprehensive tropical field program covering a wide range of interacting scales of phenomena. The purpose of this article is to provide a brief overview of EMEX. The scientific background and objective of the program, the design and execution of the experiment, and some examples and preliminary analyses of the data collected will be discussed, together with the experiments relevant to its parent program, the Tropical Ocean Global Atmosphere Program (TOGA).

2. Motivation, objectives, and background

EMEX was motivated by the continuing need for a better understanding of the relationship of convection to large-scale dynamics and climate. Of particular interest is near-equatorial convection, which occurs around the globe over both land and ocean and is an integral part of large-scale quasi-steady flow patterns such as the Hadley cell, Walker cell, the Pacific east–west circulations involved in El Niño–Southern Oscillation events, and the Asian winter monsoon. Such convection is regionally enhanced over the tropical land masses of Africa and Central America, and especially over the warm pool regions of the tropical Indian and Pacific Oceans that span Indonesia. The Indonesian region is the crossroads of the Australian-Asian summer and winter monsoons. Figure 1 presents a schematic view of the tropical circulation. For later reference, the locations of the GARP Atlantic Tropical Experiment (GATE) and the summer and winter Monsoon Experiments (summer and winter MONEX) are indicated. Over the warm-pool regions, which are persistently convective during the entire year, the total precipitation exceeds 4 m. To the north and south, over India and Australia, which possess monsoon climates with distinct wet and dry periods, the annual

* Department of Meteorology, The Pennsylvania State University, University Park, PA 16802
+ Department of Atmospheric Sciences, University of Washington, Seattle, WA 98195

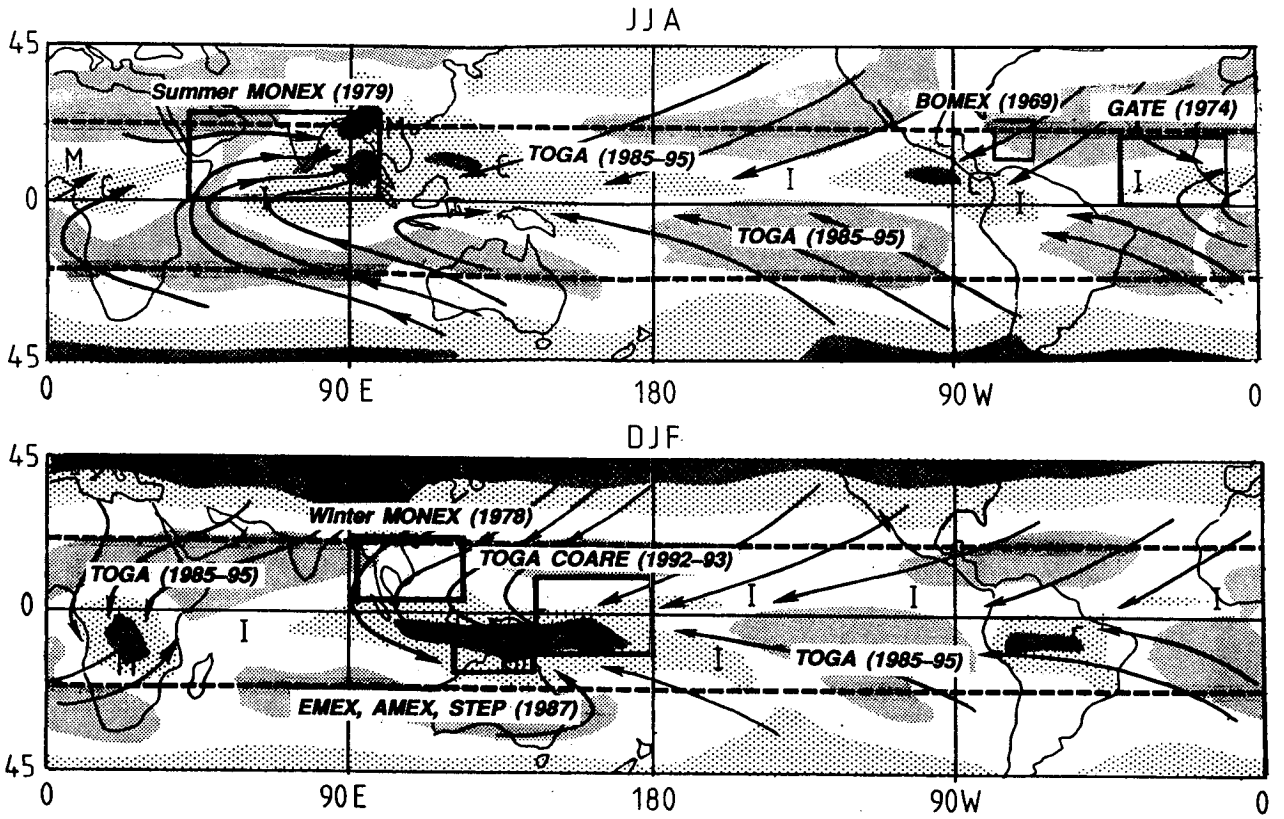

FIG. 1. Schematic view of the surface circulation of the tropics for the boreal summer (upper panel) and winter (lower panel). Contours show the long-term mean longwave radiation to space ($W m^{-2}$). Low radiating regions (OLR < 220 $W m^{-2}$) are stippled and represent regions of persistent and intense convection. The solid and dashed lines indicate the monsoonal and near-equatorial flow, respectively. The experimental domains of GATE, Summer MONEX, Winter MONEX, and AMEX/EMEX are shown as the enclosed areas. The location of the planned TOGA COARE is also indicated. Adapted from Webster (1983).

precipitation still is in excess of 2 m. Thus, over large regions of the tropics, heating budgets are dominated by latent heat release.

Large-scale modeling suggests that accurate vertical distribution of the heating associated with the cloud systems in these regions is important to the accurate calculation of the large-scale quasi-steady circulations (Hartmann et al. 1984). In particular, it was found that the large-scale circulation was extremely sensitive to the specification of the latent heating profile. Although the total heating in the column was set to be the same in each case, the response imparted by the different vertical distributions of the total heating was very dissimilar. At shorter time scales, near-equatorial oceanic mesoscale convective systems have been shown by Lau et al. (1989) to constitute an important component of the 30–60 day oscillation and of synoptic-scale westerly wind "bursts" embedded within these longer-period oscillations. These authors also emphasize the importance of the relation of the vertical distribution of heating in the cloud systems to the dynamics of the westerly wind bursts and the longer-period oscillations. Clearly, an accurate calculation or specification of the vertical heating profile is necessary for a successful simulation of the large-scale circulation.

The importance of the vertical heating profile is increased by the fact that the convection associated with the warm pools may be rapidly transmitted to higher latitudes, where it exerts a significant impact on extratropical weather. Webster and Chang (1988) and Chang and Webster (1990) have theorized that rapid communication (termed "fast" teleconnections) takes the form of modified equatorially trapped modes forced initially by periods of explosive convection in the warm pool regions. Thus, the accurate characterization of the heating function appears as a fundamental goal for a wide range of atmospheric processes. However, as recently discussed by Houze (1989), the vertical distribution of large-scale heating of the atmosphere by mesoscale convective systems in the tropics, the fundamental aggregate of the heating function, is not satisfactorily understood or documented, despite the considerable progress on this problem that has been made as a result of previous tropical field programs.

In the tropics, the large-scale averaged vertical

distribution of heating is closely related to the mean vertical distribution of vertical air motion. The statement of the First Law of Thermodynamics, scaled for low latitudes, suggests a balance between diabatic heating and adiabatic cooling, and vice versa (Charney 1969). Noting that the thermodynamic surfaces near the equator tend to be almost horizontal, it is clear that the large-scale adjustment to the heating is very rapid. Stated alternatively, the balance between diabatic and adiabatic heating and cooling is a result of a dominance of gravity-wave processes, which disperse the effects of the large-scale heating away rapidly. Thus, the problem of determining the large-scale heating reduces largely to determining the vertical air motions, which are dominated by mesoscale convective-cloud systems.

In the past ten years or so, the vertical air motions in tropical mesoscale convective-cloud systems have been inferred indirectly by various technologies. These results, however, remain somewhat inconclusive regarding such basic matters as whether the maximum upward motion (and, hence, heating) occurs in the lower, middle, or upper troposphere. As summarized by Houze (1989), the upward motion in the stratiform components of these cloud systems is undoubtedly concentrated at upper levels, while for the convective components it is unclear from the available observations whether the upward motion is concentrated in the lower, middle, or upper troposphere, or to what extent the vertical profile of convective vertical motion varies from one large-scale environment to the next.

The effects of tropical convection on horizontal momentum fields are also of interest to large-scale dynamics and climate. The coupled ocean–atmosphere system is bound by the flux of momentum from the atmosphere to the ocean and by the flux of heat and moisture from the ocean to the atmosphere. The accurate determination of these fluxes is a primary goal of the TOGA experiment and is vitally necessary for coupled ocean–atmosphere modeling. In disturbed regions of the tropics where the mean large-scale winds are small in magnitude compared to the trade-wind regime, it appears that there is a considerable enhancement of the heat, moisture, and momentum fluxes (Webster 1987). Such enhancement may result from increased gustiness associated with disturbances. Furthermore, there is evidence that momentum transport by tropical convection is highly organized when the convective cells are contained in sloping squall lines (LeMone 1983). In addition, the effects of heating and/or momentum transports by organized convection may lead to balanced mesoscale circulations, which may persist and be significant in the evolution of the atmospheric flow and precipitation. Case studies show that a mesoscale vortex can appear at midlevels in the stratiform regions of tropical convective systems (e.g., Gamache and Houze 1982, 1985; Houze and Rappaport 1984), and, of course, it is well known that tropical cyclones can develop from a mesoscale conglomerate of convection.

In view of the implications of the kinematic characteristics of tropical mesoscale cloud systems on large-scale dynamics and climate, through heating and effects on momentum and vorticity fields and the enhancement of the ocean–atmosphere interface fluxes, it would appear desirable to document as directly as possible the vertical and horizontal air motions in mesoscale convective systems. Previous documentation of vertical air motions in equatorial convection has been limited by technology. Much of the information obtained in past field studies (summarized by Houze 1989) has been inferred rather indirectly from sounding-data composites. The only extensive set of statistics on the in situ measurements of in-cloud vertical air motions in near-equatorial oceanic convective cloud systems is the set of data obtained on aircraft penetrations of clouds in GATE and analyzed by Zipser and LeMone (1980) and LeMone and Zipser (1980). Although the Zipser–LeMone studies constituted a landmark in tropical meteorology, the set of data (collected in 1974) was nonetheless limited in several respects:

- It was not comprehensive in representing all of the GATE convection, since the GATE aircraft program had several objectives, of which penetration of clouds was only one.
- No remote-sensing capability was available on the GATE aircraft, thus data could only be obtained for flight level. Since most of the GATE research flights were in the low to midtroposphere, the sampling at high levels was very limited.
- The instrumentation was suitable only for detecting intense convective vertical air motions; there was

The coupled ocean–atmosphere system is bound by the flux of momentum from the atmosphere to the ocean and by the flux of heat and moisture from the ocean to the atmosphere. The accurate determination of these fluxes is a primary goal of the TOGA experiment and is vitally necessary for coupled ocean–atmosphere modeling.

no way to obtain information in situ on the air motions in stratiform precipitation regions.

Aircraft penetration studies of convective vertical motions in the clouds of a Bay of Bengal depression during summer MONEX (Warner and McNamara 1984) and of hurricanes (Jorgensen et al. 1985) have been made with techniques and results similar to those of the Zipser–LeMone studies of GATE clouds. However, these later studies of oceanic convection have the same limitations as the Zipser–LeMone studies, and, strictly speaking, they do not describe near-equatorial oceanic convection.

The airborne studies undertaken earlier did not have the advantage of Doppler radar observational capability. However, ground-based Doppler radars have been used to document the kinematic structure of a few cases of near-equatorial continental tropical mesoscale convective systems in West Africa in great detail (e.g., Sommeria and Testud 1984; Roux et al. 1984). An excellent documentation of the structure of the squall lines that characterize many equatorial continental cloud systems over land was obtained. These studies conducted over land demonstrate the powerful ability of the Doppler radar to map the kinematic structures of these cloud systems. Documentation of equatorial oceanic cloud systems by Doppler radar, of course, could not be addressed by the studies over Africa, and the few case studies obtained do not, as yet, constitute a statistical picture of all the kinematic structures occurring over the continent.

The limitations of past datasets and the importance of having good information on the vertical velocity and other kinematic properties within equatorial cloud systems led to the primary objectives of EMEX:

- To document, as intensively and directly as possible, the vertical profile of vertical velocity and other kinematic structures of mesoscale tropical convective-cloud systems ("cloud clusters") over the ocean near the equator with the most up-to-date instrumentation available.
- To investigate the physical mechanisms responsible for the convective and stratiform components of the observed cloud systems.

The objectives were attainable primarily because of the advent of airborne Doppler research radar, which has the capability to map kinematic fields in a large atmospheric volume surrounding the aircraft remotely —not just along the flight path. The aircraft platform can cover great areas and is free to obtain Doppler radar data over the ocean. Convection over land was not studied in EMEX because the resources available for the project would not allow satisfactory documentation of both oceanic and continental cloud systems. It was considered more useful to focus on one or the other and do a good job rather than to lose focus by trying to examine both types of phenomena. Since the character of oceanic convection had not yet been explored by Doppler radar and is of interest to research connected with the El Niño–Southern Oscillation and other events over the tropical Pacific, it seemed reasonable to focus first on the oceanic cloud systems. In the remainder of the paper, we will describe how EMEX was designed and carried out as an experiment centered around airborne Doppler radar measurements to obtain a statistically meaningful sample of kinematic data in the interior of near-equatorial oceanic mesoscale convective systems. An overview of the project, a summary of the weather situations encountered, a description of the data collected, and some preliminary results indicating the successful achievement of the stated objective will be given.

3. Design and execution of the experiment

a. Location of the project

The region where EMEX was conducted is shown in Fig. 2. Large precipitation-producing cloud clusters occur throughout the equatorial latitudes, and, in principle, EMEX could justifiably have been conducted in a variety of locations. The region north of Australia, however, is ideal, since it is part of the "maritime continent," which is the name given by Ramage (1968) to the highly convective region comprised of the islands, peninsulas, and intervening seas of Indonesia, Malaysia, Papua New Guinea, and northern Australia. As pointed out by Ramage, the latent heat released in clouds and precipitation in this region during the austral summer constitutes one of the primary sources of energy for the atmosphere. In addition, the tropopause is higher and colder here than anywhere in the atmosphere at any time and is representative of other monsoon regions during their convective phases and the tropical atmosphere over the tropical ocean warm pools. To illustrate the ubiquity of the convection in the region, Fig. 3 shows a comparison of the vertical profiles of heating from a number of regions in the tropics. With the exception of the GATE profile, the AMEX heating rates (W. Frank, personal communication) match those from the western Pacific and Atlantic Oceans.[1] Hence, the cloud clusters that occur in this region are of considerable general interest and an ideal target for a study of tropical convection.

[1] The locations of the profiles can be seen in Fig. 1. The western Pacific profiles are indicative of the TOGA COARE region.

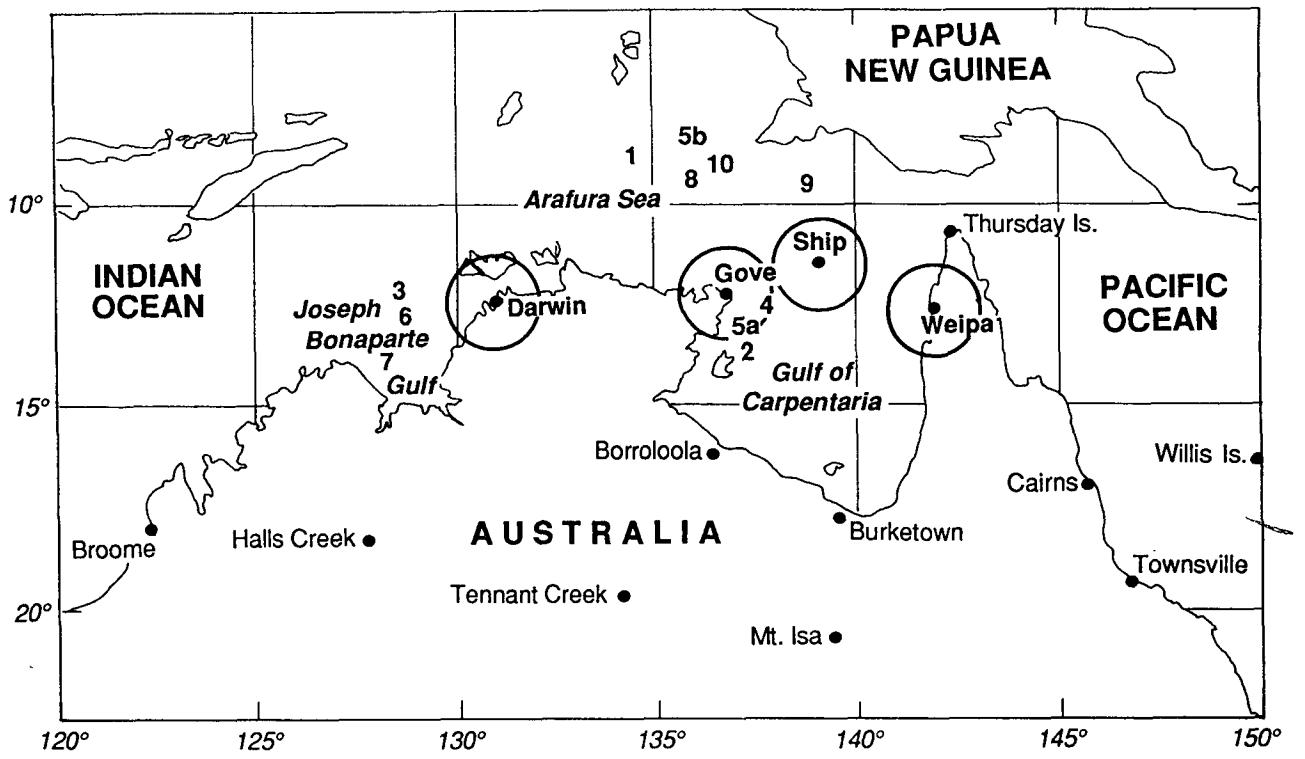

FIG. 2. Detailed domain of AMEX and EMEX. The special AMEX sounding stations are indicated by large dots. The locations of AMEX land-based radars and the TOGA radar, the latter based on a PRC ship, are surrounded by circles of 100-km radius. The plotted numbers refer to the ten flights of the P3 aircraft during EMEX, details of which are given in the text and Table 1. The location of each number denotes the general location of the cloud system investigated on that day. EMEX flight 5 investigated two systems, labeled 5a and 5b.

AMEX and STEP were also being conducted simultaneously with EMEX and were also taking advantage of the intense convection in the North Australia–Indonesia region. Thus, a clear opportunity was provided to document the cloud clusters in a particularly interesting region in an intensified observational setting. EMEX was headquartered along with AMEX and STEP in Darwin. Operational centers for all three programs were located in the Bureau of Meteorology forecast office in Darwin. The Royal Australian Air Force base at Darwin was the primary base for the EMEX and STEP aircraft operations, with Gove on the northwest corner of the Gulf of Carpentaria (see Fig. 2) providing a secondary base.

b. Facilities

As noted above, the primary objective of EMEX was to document the kinematics of tropical cloud clusters as directly as possible, and the most effective way to accomplish that objective technologically was with airborne Doppler radar. Hence, EMEX was organized with airborne Doppler radar as the primary facility. The only facility of this type in the world available at the time of EMEX was aboard a U.S. National Oceanic and Atmospheric Administration (NOAA) long-range WP3D aircraft (referred to hereafter as the P3). Under the operating conditions of EMEX, this aircraft had a maximum flight duration of about 10 h. Two other moderately long-range aircraft were also employed, to provide flight-path wind data to confirm and extend the airborne Doppler data and to provide essential thermodynamic data to accompany the kinematic data. These were the U.S. National Center for Atmospheric Research (NCAR) Electra and the Australian Commonwealth Scientific Industrial Research Organization (CSIRO) F27, which had mission durations of approximately 8 and 6 h, respectively. In addition to these three aircraft, the STEP aircraft, which was the U.S. National Aeronautics and Space Administration (NASA) ER-2, occasionally coordinated its high-altitude missions (near the tropopause, at and above cloud top) with those of the EMEX aircraft, which flew in the mid- to low-troposphere. When missions were flown in the eastern part of the EMEX area (i.e., over the Gulf of Carpentaria or Arafura Sea) the F27 aircraft, because of its shorter range, operated out of Gove. Otherwise, all the aircraft were based at and operated out of the Royal Air Force base in Darwin.

In addition to the aircraft, a shipborne platform was provided to EMEX. The ship was the People's Repub-

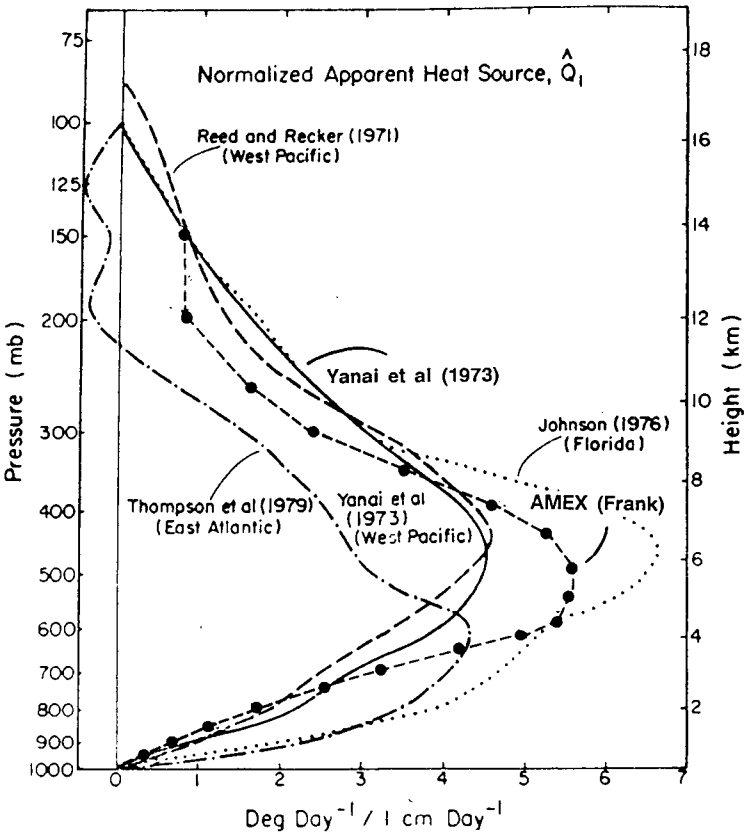

FIG. 3. A comparison of the vertical profiles of heating from the GATE in the eastern Atlantic Ocean (Thompson et al. 1979), the western Pacific (dashed, Reed and Recker 1971; solid, Yanai et al. 1973), Florida (dotted, Johnson 1976), and northern Australia–Indonesia (AMEX, Frank, personal communication). The curves are all normalized to a common precipitation rate of 10 mm d^{-1}. Note the similarity of all profiles except the GATE profile, which possesses a much lower heating maximum.

lic of China (PRC) Research Vessel *Xiang Yang Hong No. 5*. It was located in the Gulf of Carpentaria, where it would best supplement the AMEX sounding and radar arrays (Fig. 2). The vessel was equipped with upper-air sounding equipment and a U.S. NOAA/TOGA C-band Doppler weather radar.

The instrumentation aboard the EMEX aircraft is described by Gamache et al. (1987). Each aircraft carried a complement of sensors for measuring the standard thermodynamic and wind variables as well as radiation and cloud-physics parameters. The P3 aircraft also had the ability to launch dropwindsondes. The key instruments for this project, however, were the C-band (5-cm wavelength) lower-fuselage radar and the X-band (3-cm wavelength) tail Doppler radar on board the P3. The lower-fuselage antenna, mounted below the aircraft, swept 360° in the horizontal, detecting the horizontal pattern of radar reflectivity produced by precipitation. At the same time, the tail radar continuously provided vertical cross sections through the precipitation pattern. Its antenna pointed normal to the aircraft's ground track and swept circularly through 360° ten times per minute. The lower-fuselage radar measured only reflectivity. The tail radar measured both reflectivity and the mean velocity of the precipitation particles along the beam of the radar.

c. Flight program

The three EMEX aircraft were used exclusively to penetrate mesoscale cloud systems and document their kinematic structure. This mode of operation prevented the observational program from being defocused by a series of secondary objectives. The basic premise of the experimental design was that the scientific objectives would best be met by a semistatistical dataset obtained by repeated sampling of cloud clusters in an identical manner during as many missions as possible. Moreover, it was recognized a priori that, because of inevitable errors in forecasts of cloud cluster location and timing, aircraft operating constraints, possible instrumental failures, and other practical considerations, every attempt to penetrate and measure the kinematic properties of a cluster would be somewhat less than perfect. It was thus deemed important to concentrate on the main objective, trying repeatedly to document the kinematic structure of cloud clusters by direct penetration. Every aircraft-mission opportunity was thus used to contribute to this basic objective.

The same basic flight strategy was used in every mission so that the data would be collected consistently from case to case. This strategy is summarized in Figs. 4 and 5, which show, in idealized form, the manner in which the EMEX aircraft were flown in each cloud cluster that was investigated. These diagrams are taken from the flight-planning document written prior to the actual experiment (Marks 1986). It is a tribute to this plan that every EMEX aircraft mission was a successful adaptation of this plan to a particular case. Figure 4 shows the plan followed by the P3, while Fig. 5 shows the plan followed by the Electra and F27 aircraft, which always flew in coordination with the P3.

A basic premise of the aircraft plan was that the precipitation pattern within a cloud cluster would exhibit a precipitation pattern that consisted partly of a line or lines of convection and partly of an area of stratiform precipitation. Such structure would be consistent with past studies of tropical cloud clusters

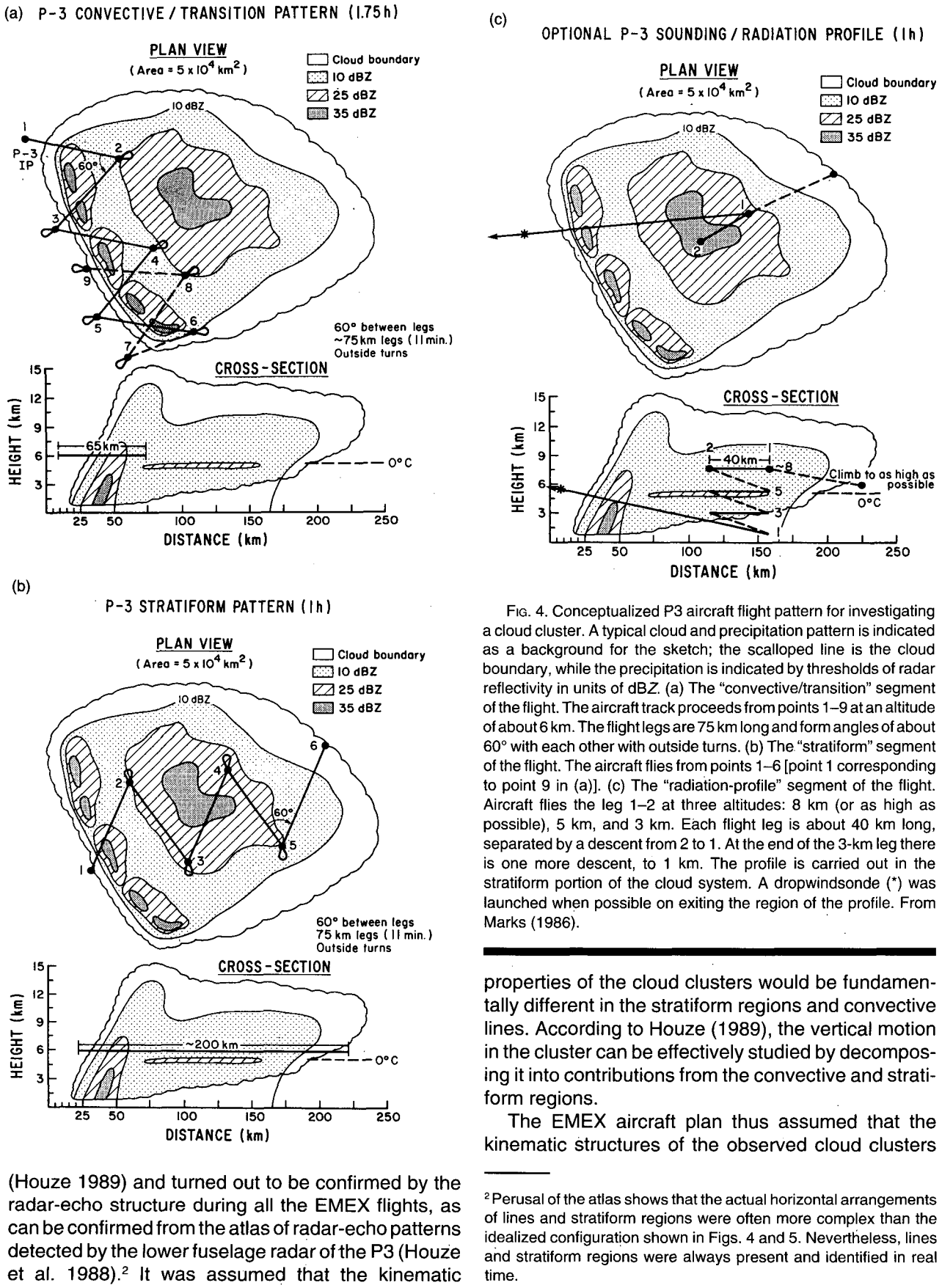

FIG. 4. Conceptualized P3 aircraft flight pattern for investigating a cloud cluster. A typical cloud and precipitation pattern is indicated as a background for the sketch; the scalloped line is the cloud boundary, while the precipitation is indicated by thresholds of radar reflectivity in units of dBZ. (a) The "convective/transition" segment of the flight. The aircraft track proceeds from points 1–9 at an altitude of about 6 km. The flight legs are 75 km long and form angles of about 60° with each other with outside turns. (b) The "stratiform" segment of the flight. The aircraft flies from points 1–6 [point 1 corresponding to point 9 in (a)]. (c) The "radiation-profile" segment of the flight. Aircraft flies the leg 1–2 at three altitudes: 8 km (or as high as possible), 5 km, and 3 km. Each flight leg is about 40 km long, separated by a descent from 2 to 1. At the end of the 3-km leg there is one more descent, to 1 km. The profile is carried out in the stratiform portion of the cloud system. A dropwindsonde (*) was launched when possible on exiting the region of the profile. From Marks (1986).

(Houze 1989) and turned out to be confirmed by the radar-echo structure during all the EMEX flights, as can be confirmed from the atlas of radar-echo patterns detected by the lower fuselage radar of the P3 (Houze et al. 1988).[2] It was assumed that the kinematic properties of the cloud clusters would be fundamentally different in the stratiform regions and convective lines. According to Houze (1989), the vertical motion in the cluster can be effectively studied by decomposing it into contributions from the convective and stratiform regions.

The EMEX aircraft plan thus assumed that the kinematic structures of the observed cloud clusters

[2] Perusal of the atlas shows that the actual horizontal arrangements of lines and stratiform regions were often more complex than the idealized configuration shown in Figs. 4 and 5. Nevertheless, lines and stratiform regions were always present and identified in real time.

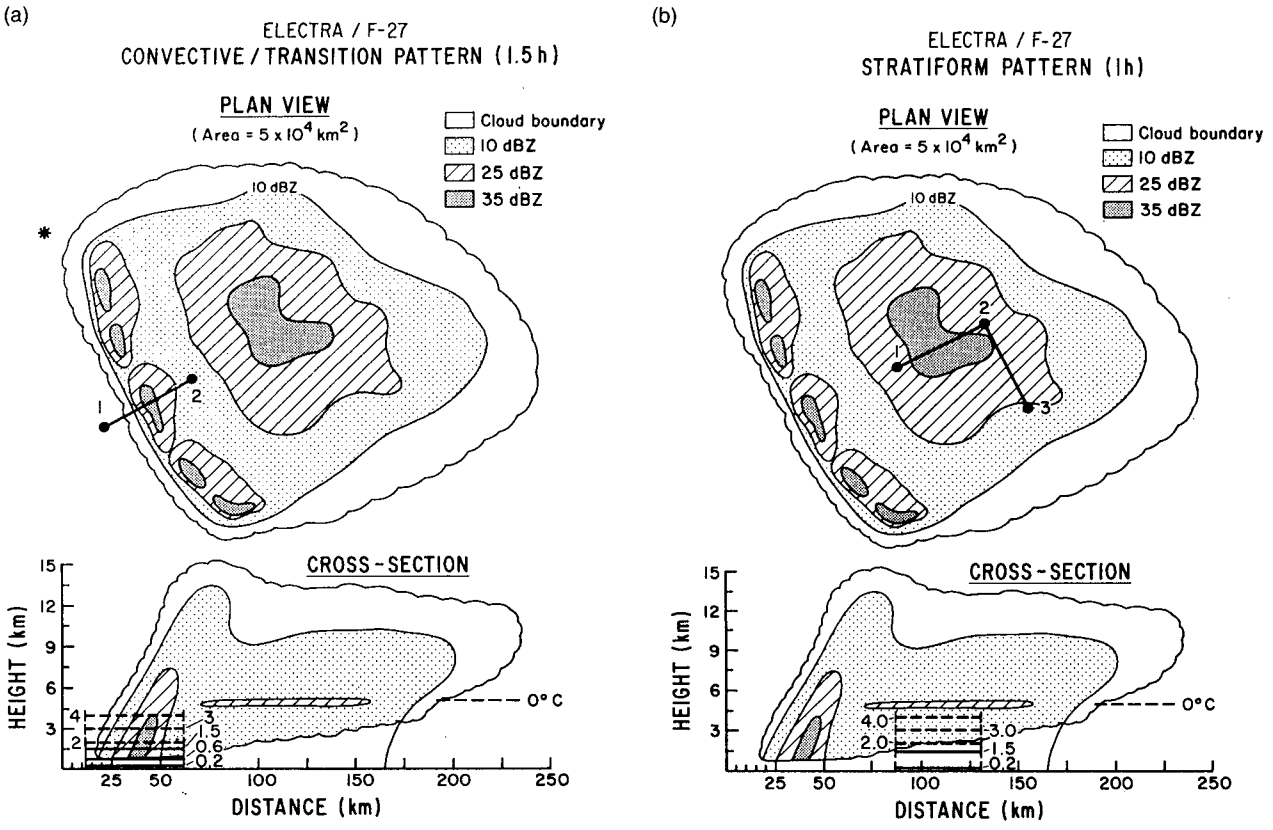

FIG. 5. Conceptualized F27 and Electra aircraft flight patterns for investigating a cloud cluster. A typical cloud and precipitation pattern is indicated as a background for the sketch; the scalloped line is the cloud boundary, while the precipitation is indicated by thresholds of radar reflectivity in units of dBZ. (a) The "convective/transition" segment of the flight. The aircraft track proceeds back and forth between points 1 and 2, which are 50 km apart. This track lies below the zone in which the P3 flies. (b) The "stratiform" segment of the flight. Aircraft flies pattern 1–2–3 at two altitudes. In both (a) and (b), the Electra and F27 aircraft fly one above the other at a series of altitudes in the lower troposphere. From Marks (1986).

could best be reconstructed by focusing one portion of the flight on the convective line(s) and another portion on the stratiform region. The first part of each P3 aircraft mission, after ferrying to the location of the cloud cluster to be investigated, was a survey to locate the principal convective lines and stratiform region. During the survey several dropwindsondes were launched to document the immediate environment of the cloud system. After the survey, the P3 aircraft scientist usually organized the subsequent parts of the mission and coordinated and directed the Electra and/or F27 into position for the convective and stratiform components of the mission.

The convective portion of the flight (Figs. 4a and 5a) was actually referred to as the "convective/transition pattern," since this portion of the flight was expected to and did sample many convective cells that were undergoing transition from convective to stratiform structure. In the convective/transition pattern, the P3 flew a zigzag pattern repeatedly across the convective line, progressing from one end of the line to the other and back. Pseudodual Doppler radar analysis uses the data obtained by the tail radar (which points normal to the flight track) at points interior to each V formed by the flight track.[3] The wind component measured along the beam normal to one of the two flight legs forming the V is combined with the wind component normal to the other leg of the V. If the angle of the V is large enough, the horizontal wind and its divergence can be reconstructed reliably. The choice of 60° for the angle of the V optimizes the amount of area covered by dual-Doppler measurements, which increases as the angle decreases toward zero, and optimizes the reliability of the wind estimates obtained by combining the data from the two flight legs, which increases as the orthogonality of the flight legs increases (Marks 1986). While the P3 flew in its zigzag pattern at midlevels, collecting dual-Doppler radar data and making other measurements, the Electra and/or F27 flew back and forth across the line at a series of altitudes in the low troposphere (Fig. 5a).

In addition to being useful in a dual-Doppler mode

[3] Actually, some points exterior to the V are also used.

of observation, the data collected with the tail Doppler radar provided a high-resolution time–height section of reflectivity and particle velocity along the flight track. This cross section was obtainable since, as noted in section 3b, the antenna of the tail radar sweeps rapidly through 360° of elevation whenever it is operating. In contrast to the dual-Doppler analysis, which is constructed from the elevation angles that have a substantial horizontal component, the time–height section is constructed from the rays of data collected whenever the antenna points directly upward or downward. We refer to the data in the time–height section as "vertical incidence" data, indicating that it is constructed from these purely vertically pointing rays.

The stratiform portion of the mission consisted of a zigzag Doppler radar pattern by the P3 across the entire breadth of the stratiform region (Fig. 4b), while the Electra flew a series of shorter horizontal legs at various levels in the lower troposphere (Fig. 5b).

The final phase of the mission was a "radiation profile" obtained by the P3 in the stratiform region. It had been hypothesized that an important part of the diabatic heating of the large-scale environment by a cloud cluster arises as a result of the divergence of net radiative fluxes in the cloud system (Webster and Stephens 1980; Houze 1982). To document the columnar radiative flux divergence as much as possible, the aircraft, which carried a full complement of radiation and cloud-physics instrumentation, ascended to its maximum operating altitude (usually about 7–7.5 km) and descended in stages to the low troposphere to measure the vertical profiles of long and shortwave radiative fluxes (Fig. 4c). The Electra and F27 did not participate in this part of the flight pattern.

d. Daily mission planning

The EMEX aircraft were available for use in the project from early January to mid-February. During this period, a daily cycle of planning was carried out to decide whether or not to organize an aircraft mission and, if so, when and where it should be carried out. These decisions had to be carefully weighed each day, since the aircraft were available for use in a total of only ten full-duration multiple-aircraft missions. In order to make decisions on use of the aircraft carefully and systematically, the synoptic weather situation was monitored and forecast at the project headquarters in Darwin by Mark Williams of the Australian Bureau of Meteorology. At 2100 LST each day, the EMEX scientific and aircraft operational staffs held a 1-h meeting chaired by a collectively agreed-upon mission scientist for that day. A weather briefing and forecast were presented by Williams, the status of each of the research facilities was reported, and input from the STEP and AMEX scientists was received. A brief, open discussion of the overall situation then led to a recommendation concerning whether a mission should be organized and in what part of the EMEX region it would best be conducted. The EMEX principal investigators[4] then decided among themselves, based on all of the available input, whether or not to carry out a mission. If the decision was to go ahead with the mission, they conveyed this action to the mission scientist who continued to monitor the weather situation until about midnight, at which time the final decision was given to the aircraft operational personnel. Takeoff of the first aircraft was typically 0200–0400 LST (1700–1900 UTC). The reason for the early morning takeoff was the diurnal modulation of the mesoscale convective systems, which systematically favored the development of oceanic cloud clusters during the midnight-to-sunrise period. This nocturnal characteristic appears typical of the oceanic regions lying between the land masses of the maritime continent (Williams and Houze 1987).

e. Summary of aircraft missions

The aircraft missions conducted in EMEX are listed in Table 1 with some basic information about each flight. Altogether there were ten missions, designated EMEX1, EMEX2, etc. All missions were conducted with multiple aircraft. In one case there were four aircraft, in seven cases there were three aircraft, and in two cases there were two aircraft. The airborne Doppler radar on the P3 functioned on all ten flights with only occasional minor difficulties. Indeed, instrumentation systems on all the aircraft functioned nearly flawlessly.

The P3 aircraft, with its radar instrumentation, functioned as the lead aircraft in all ten missions. In every case, the P3 was accompanied by the F27 and/or the Electra, so that coordinated flight plans of the types illustrated in Figs. 4 and 5 could be executed. As a result of excellent forecasting and careful choice of regions to investigate during the daily planning meetings, a significant mesoscale convective-cloud system was successfully intercepted by the aircraft on every mission. Each mesoscale convective system was comprised of an evolving pattern of convective lines and stratiform precipitation, which could be identified in real time with the P3 radars. It was therefore possible for the airborne mission scientist on the P3 to direct the flight plan with respect to the convective and stratiform areas identified in real time. It was possible in all ten flights to map out and execute each of the three successive phases of the flight plan (convective-

[4] A list of principal investigators and scientists is given in appendix A.

TABLE 1. Mission specifications.

Mission	Date (1987)	Aircraft	Data Period: UTC (LST)	Location	850-mb Flow Pattern
EMEX1	14–15 Jan	P3, Electra, F27	1800–2400 (0200–0800)	Arafura Sea	Northwesterly flow between New Guinea and Australian vortices
EMEX2	15–16 Jan	P3, Electra, F27	1900–0100 (0300–0900)	Gulf of Carpentaria	Col at east end of northwesterly flow between New Guinea and Australian vortices
EMEX3	16–17 Jan	P3, Electra	1930–0100 (0330–0900)	Joseph Bonaparte Gulf	Northwesterly flow between New Guinea and Australian vortices
EMEX4	18–19 Jan	P3, Electra, F27	1830–0000 (0230–0800)	Gulf of Carpentaria	Tropical Cyclone Irma
EMEX5a	19–20 Jan	P3, Electra, F27	1900–2100 (0300–0600)	Gulf of Carpentaria	Tropical Cyclone Irma
EMEX5b	19–20 Jan	P3, Electra, F27	2100–0100 (0600–0900)	Arafura Sea	Northwesterly flow between New Guinea and Australian vortices
EMEX6	27–28 Jan	P3, Electra, F27	1900–0030 (0300–0830)	Joseph Bonaparte Gulf	Near center of Australian vortex
EMEX7	29–30 Jan	P3, Electra, F27	1800–0030 (0200–0830)	Joseph Bonaparte Gulf	Southwesterly flow on northwest side of Australian vortex
EMEX8	1–2 Feb	P3, Electra, F27	1830-0030 (0230-0830)	Arafura Sea	Westerly flow between New Guinea and Australian vortices
EMEX9	2–3 Feb	P3, Electra, F27 ER2	1900–0030 (0300–0830)	Arafura Sea	Westerly flow between New Guinea and Australian vortices
EMEX10	3–4 Feb	P3, F27	2000–0100 (0400–0900)	Arafura Sea	Northwesterly to southwesterly flow between New Guinea and Australian vortices

transition, stratiform, and radiation profile) in relation to the real precipitation areas in a manner very similar to the idealized plans shown in Figs. 4 and 5.

The location of the center of the area within which each of the research flights was executed is indicated in Fig. 6. These flights were conducted in three oceanic locations: the Joseph Bonaparte Gulf, the Arafura Sea, and the Gulf of Carpentaria. It had been hoped that most of the flights could be conducted over the Gulf of Carpentaria where the AMEX upper-air sounding system and the shipborne Doppler radar were located. However, the cloud systems were rarely located in that region at the times that flights could be carried out and, therefore, had to be sampled where they actually occurred. The location of each flight with respect to the prevailing meteorological situation, as indicated by the winds at the 850-mb level, is also listed in Table 1 and will be elaborated on in the next section.

4. Large-scale weather patterns during the flight program

a. The timing of EMEX: The specter of El Niño

The long-term average circulation of the winter monsoon (Fig. 1) is subject to considerable interannual variability. In the north Australian–Indonesian region,

there is a very strong correlation between the rainfall of the winter monsoon and the Southern Oscillation Index (SOI).[5] The SOI is a keen indicator of the existence of an El Niño period, which is generally associated with anomalously low rainfall over north Australia, at least averaged over the summer wet season. The correlation between seasonal rainfall and the SOI is very high. However, determining whether or not one month of a wet season will be above or below average, even during an El Niño event, is a difficult task.

Figure 6a shows that the SOI was anomalously low, indicating that January and February 1987 were well within an El Niño period. Figure 6b shows the January Darwin-Daly district rainfall from 1955 to 1986. The shaded bars represent El Niño years. There had been earlier indications that the 1986/87 winter would be an El Niño, which might have allowed some flexibility in the planning. However, given that the forecasts were for a weak or moderate El Niño, far weaker than the 1982/83 episode, as the logistics of the experiment were already in place and as STEP and AMEX had decided to proceed in any event, EMEX was implemented. The hatched bar of Fig. 6b represents the rainfall that actually fell in the Darwin-Daly district. Despite the El Niño, the month of January turned out to be one of the wettest on record!

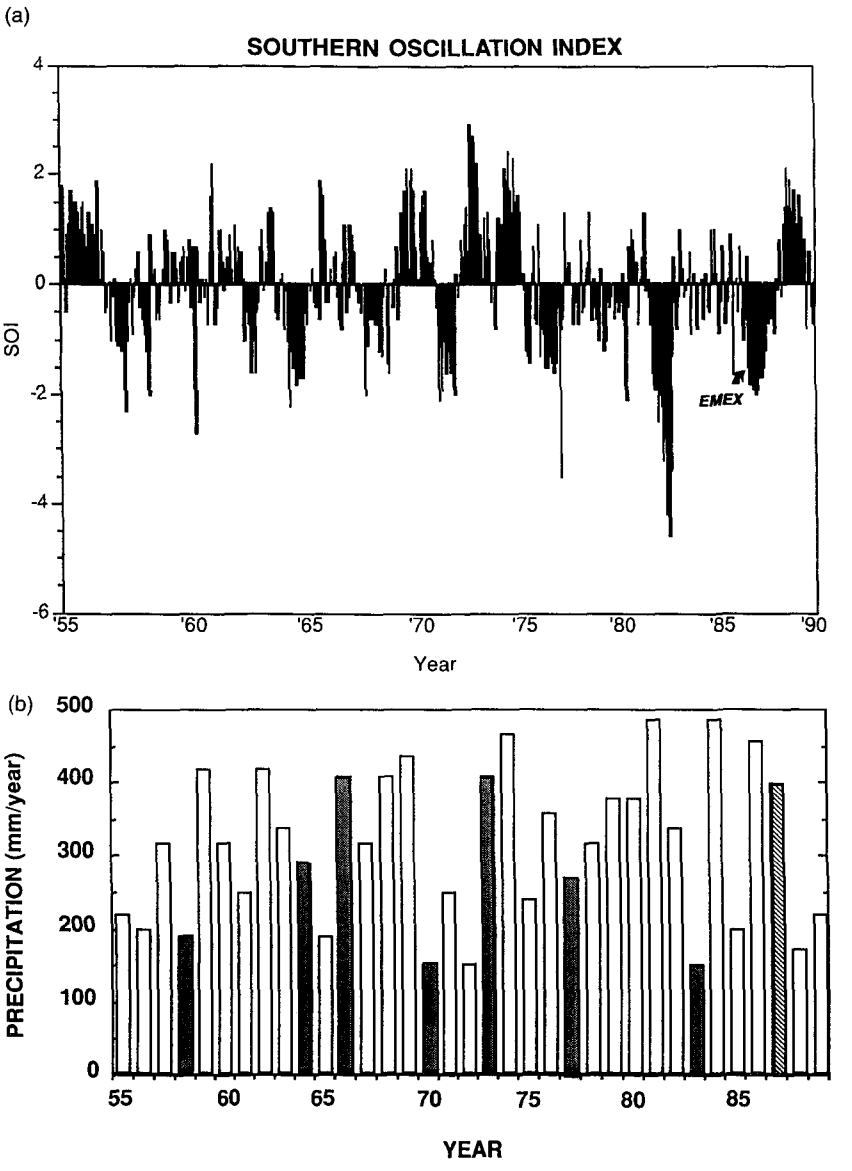

FIG. 6. (a) The Southern Oscillation Index (SOI) plotted as a function of time. (b) The mean rainfall for the Darwin-Daly rainfall district. Years of SOI << 0 (i.e., El Niño years) are shaded. The hatched bar, also an El Niño year, represents the mean district rainfall during the January of EMEX.

b. Large-scale context of the EMEX period

Figures 7a and b show the time–latitude section of the 850-mb wind between 60°E and the date line along 10°S, and the equator for the period 1 December through 28 February. Easterly winds are shown as dashed contours and westerlies as solid contours. The longitudinal and temporal limits of the EMEX experiment are defined by the heavy solid lines. Along the right-hand ordinate, the active periods[6] A1, A2, and A3 of the northwest monsoon are indicated for later reference. Along the equator (Fig. 7a) the lower tropospheric winds may be categorized into two main periods. Prior to the EMEX period, the equatorial winds were primarily westerly to the east and over the EMEX longitudes. The occasional increases in intensity of the westerlies correspond to "westerly bursts" (WCRP 1990). During the EMEX time frame, the winds remained easterly. Along 10°S (Fig. 7b), the

[5] The SOI is essentially the sea level pressure difference between Tahiti and Darwin and provides an indication of the macro-scale dynamic influences existing on the EMEX region.

[6] The definition of "active" phase of the monsoon as used by the Darwin regional office of the Australian Bureau of Meteorology is used. An active period occurs when the 850-mb westerly wind in the box 110°–140°E, 5°–15°S exceeds 8 m s^{-1}.

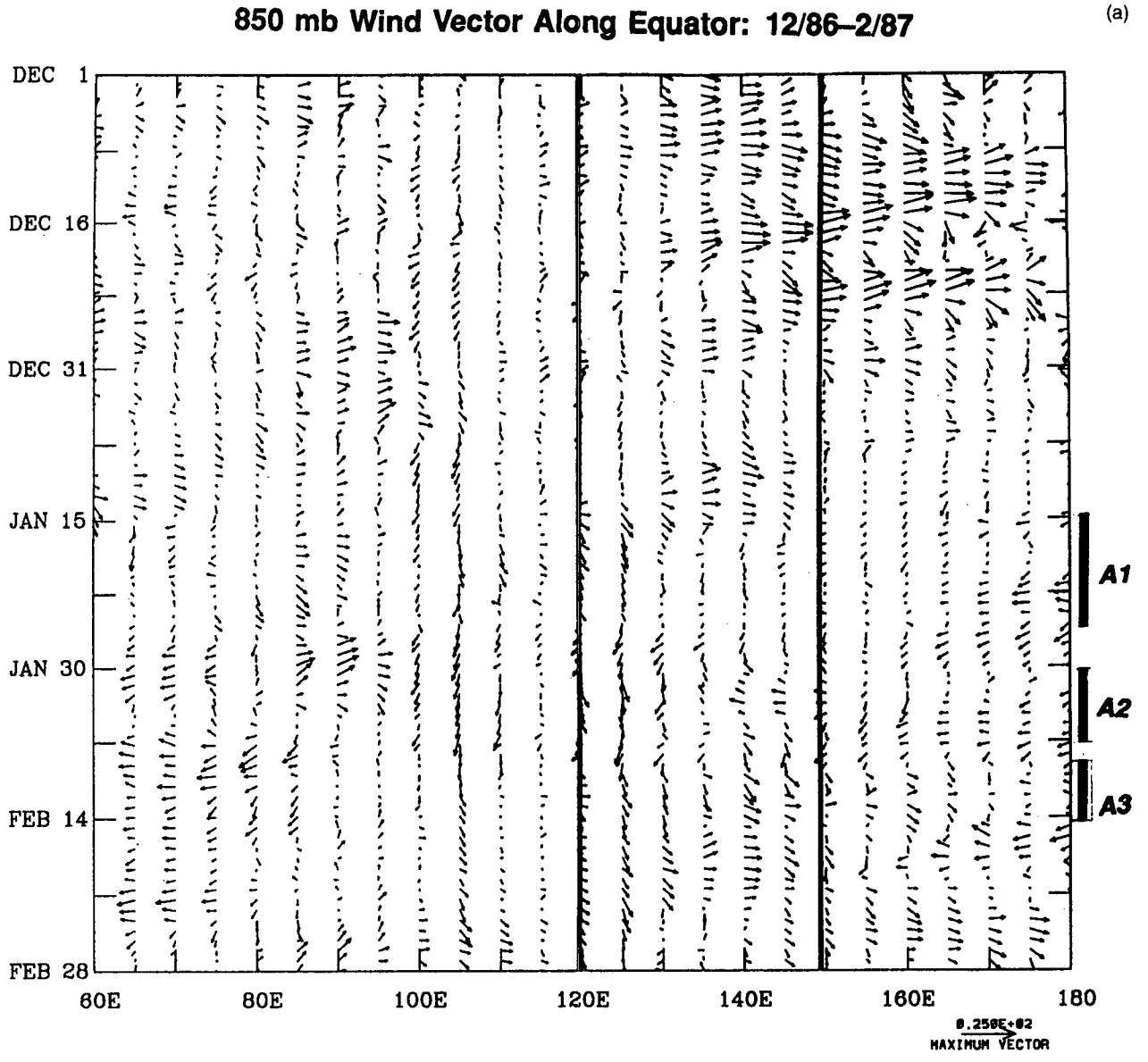

FIG. 7. (a) Time–longitude section of the 850-mb zonal wind component along the equator. Easterly winds are dashed and westerly winds are solid. Horizontal lines labeled A1, A2, A3 denote the three active periods in EMEX. The two vertical lines define the longitudinal extent of the EMEX area. Vector to the lower right of the diagram indicates the magnitude of a 20 m s^{-1} wind.

winds are almost completely reversed compared to the winds along the equator. Easterlies dominated throughout December and early in January. After 14 January, the westerly winds increase considerably and three active periods (A1, A2, and A3) developed where westerly winds exceeded 20 m s^{-1}. These occur with the establishment of the northwest monsoon over north Australia. Once established, the monsoon extended from 90°E to 150°E during A1 and even further eastward during the second two active periods. A3, however, was limited to the EMEX domain and to the east. Clearly, the westerlies of the monsoon were planetary in scale.

c. Progression of the weather pattern in the EMEX domain

The progression of weather situations over the AMEX/EMEX area is summarized by the zonal-wind time cross section in Fig. 7c, where the periods of 850-mb westerly wind in excess of 8 m s^{-1} over the region 110°-140°E, 5°–15°S are designated as "active" monsoonal periods. The days on which EMEX aircraft missions were conducted are also indicated in the plot as EMEX1, 2, etc.

The sequence of winds at 850 mb bears a noticeable relation to monsoonal precipitation over the AMEX/EMEX region. The Darwin rainfall, plotted in Fig. 8,

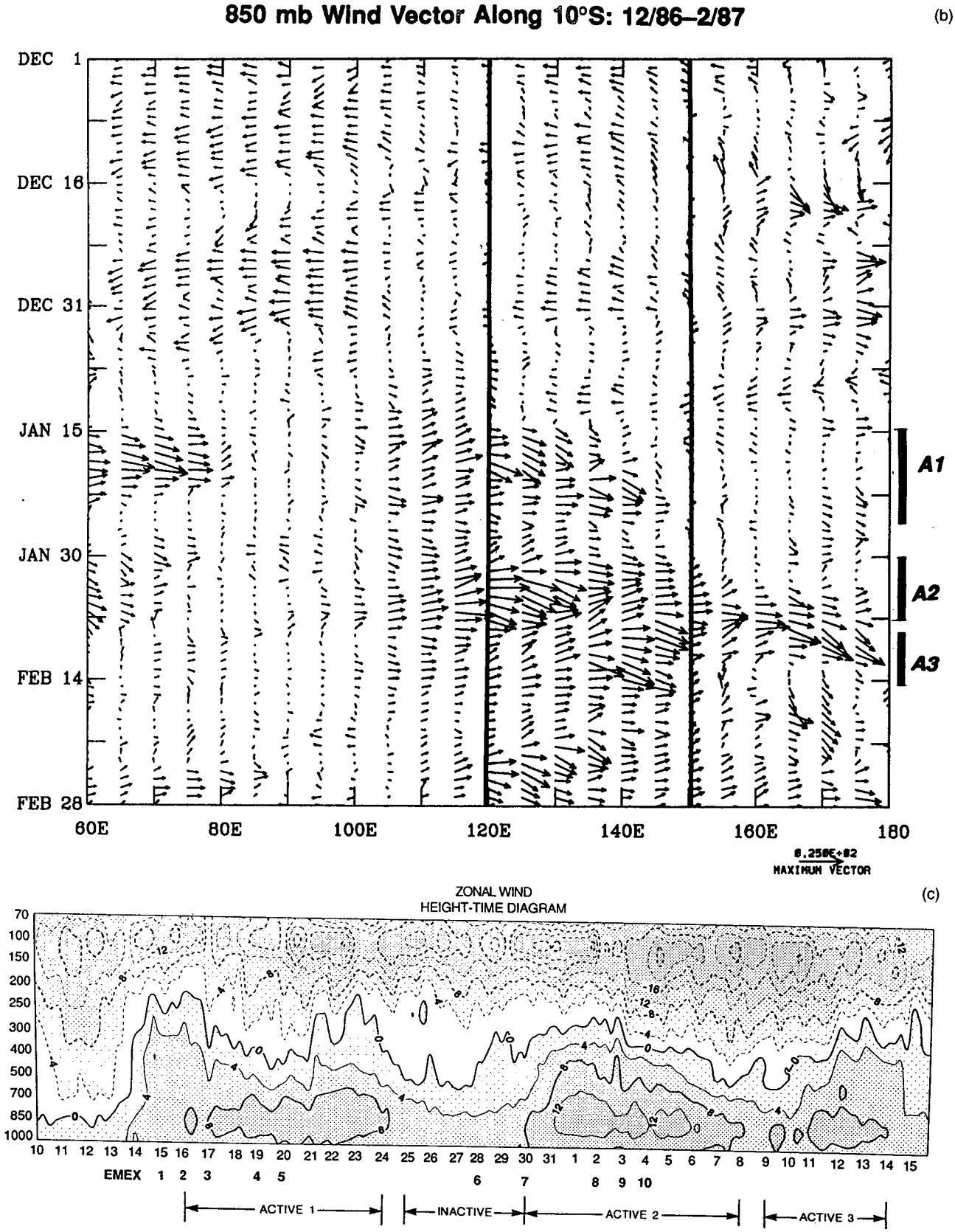

FIG. 7.(b) Same as (a) but along 10°S. (c) Area mean values of the zonal-wind component over the region 110°E to 140°E, 5°S to 15°S. Based on uninitialized analyses (6 hourly) starting 10 January 1987. The notation EMEX 1, 2,...10 refers to the ten EMEX aircraft missions. Starting data is 10 January 1989. Adapted from Heckley and Puri (1988).

was heavy during the two active periods. Close inspection of the rainfall sequence reveals, however, that the precipitation periods began as the winds at 850 mb began to increase (i.e., a few days before the mean 850-mb wind reached the 8 m s^{-1} threshold defining the active period). Also, in the case of the A1 active period, the rain decreased and stopped before the westerlies died down.[7] This halting of the rain was associated with a significant change in the circulation pattern, which resulted in a change of the westerly flow from moist maritime to dry continental.

The sequence of synoptic situations associated with the progression of the monsoon during the period of EMEX aircraft missions is better understood by noting the mean flow pattern over the region at 850 mb during the period of the experiment shown in Fig. 9a. The monsoonal westerlies occurred north of the semi-permanent Australian Low located at about 18°S, 119°E and the monsoon trough, which extended roughly east–west across Australia. The position and strength of the westerlies varied as the Australian Low underwent slow temporal and spatial variations. The strength of the westerlies also varied in connection with other synoptic-scale vortices, which formed and dissipated but were not persistent enough to be evident in the mean flow pattern. The mean high cloud amount distribution for the same period is shown in Fig. 9b. High cloud is seen to predominate over the northern part of Australia and is clearly associated with the strong confluent pattern.

One of these other synoptic-scale features was a counterclockwise rotating vortex located on the equator near New Guinea (referred to hereafter as the New Guinea Vortex). The Australian Low and the New Guinea Vortex together often formed a vortex pair, whose position during the period A1 was typified by that seen in Fig. 10a. This vortex appeared north of New Guinea (at about 1°N, 145°E) on 13 January, which can be seen from Fig. 6c to coincide with the beginning of the strengthening of the westerlies leading up to the period A1. The inception of the strengthening westerlies occurred at about the same time the activity of mesoscale convective systems in the EMEX area began to increase and large amounts of precipitation began to fall in Darwin (Fig. 8). The first decision to carry out an aircraft mission was made during this period (see EMEX1, Table 1 and Fig. 6c). After its formation, the New Guinea Vortex moved slowly westward, reaching the west end of the island on 16 January, where it remained stalled in roughly the position shown in Fig. 10a until it disappeared on 18 January. The strong northwesterly flow between this New Guinea Vortex and the Australian Low is the

[7] The precipitation peak at Darwin on 21 January was rather local, unrepresentative of the broader region surrounding Darwin. This fact is evident from inspection of the Darwin radar data (Keenan and Martin 1987).

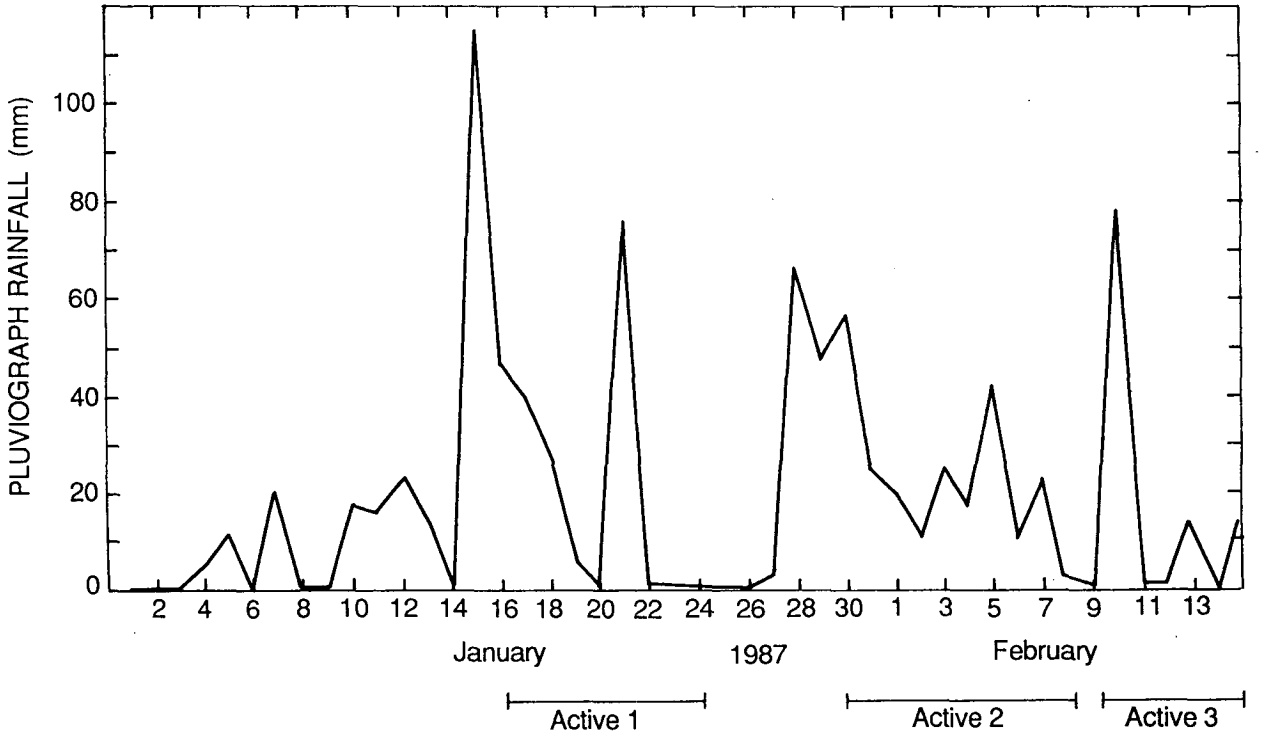

FIG. 8. Twenty-four-hour area integrated rainfall amounts from Bureau of Meteorology pluviograph for the Darwin region.

feature largely responsible for the increased westerlies during A1. The first three EMEX aircraft missions (EMEX1, 2, and 3) were conducted while the pattern resembled that in Fig. 10a. EMEX3 was carried out over the Bonaparte Gulf (Fig. 3) at the time of Fig. 10a.

About one-third of the way through A1, on 19 January, a tropical cyclone (hurricane) named Irma formed in the Gulf of Carpentaria (Fig. 10b). Thus, for a time, the synoptic situation was dominated by three closed circulations: The Australian Low, the New Guinea Vortex, and Irma. The EMEX4 aircraft mission was conducted in Irma during this period (Fig. 2 and Table 1). On 20 January, the New Guinea Vortex disappeared, leaving only the Australian Low and Irma (Fig. 10c). EMEX5, conducted on this day (Fig. 8c, Table 1), investigated both the center of Irma (EMEX5a) and the monsoonal westerly inflow (EMEX5b). After landfall on 20 January, Irma degenerated to a weaker but persistent vortex, which moved southward toward the center of Australia. After 20 January, the Australian Low began moving toward an anomalously southward position over land and gradually weakened. As a result of these changes, the westerlies during the later part of A1 became dry (Fig. 8), then weakened, and the "inactive" period between A1 and A2 indicated in Fig. 6c prevailed for several days.

During the inactive period, a new Australian Low formed over Arnhem Land, on the northern peninsula where Darwin is located. On 28 January, a new New Guinea Vortex formed on the equator at about 142°E (Fig. 10d). This location is very near where the first New Guinea Vortex had formed. This second New Guinea system followed a

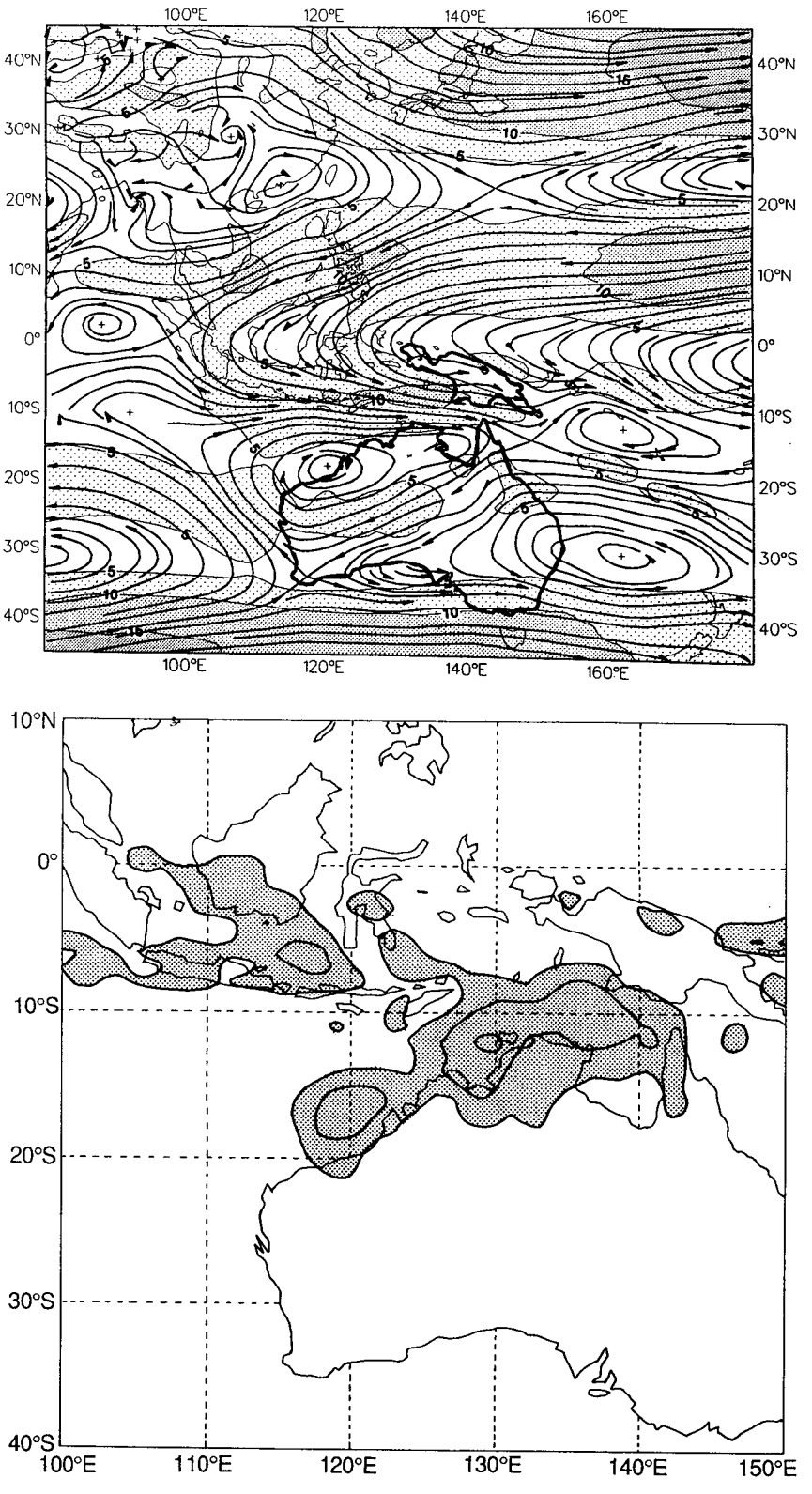

FIG. 9 (a) Time-averaged flow at the 850-hPa level for the period covering 10 January—15 February 1987. Only data from 0000 UTC are included in the average. Streamlines and isotachs (10 m s^{-1} intervals) are shown. Coastlines of Australia and the island of New Guinea are darkened. Adapted from Heckley and Puri (1988). (b) Time-averaged OLR satellite data for the period 14 January—4 February 1987. Contours (every 10%) show the percent of time that the equivalent infrared temperature was < −55°C.

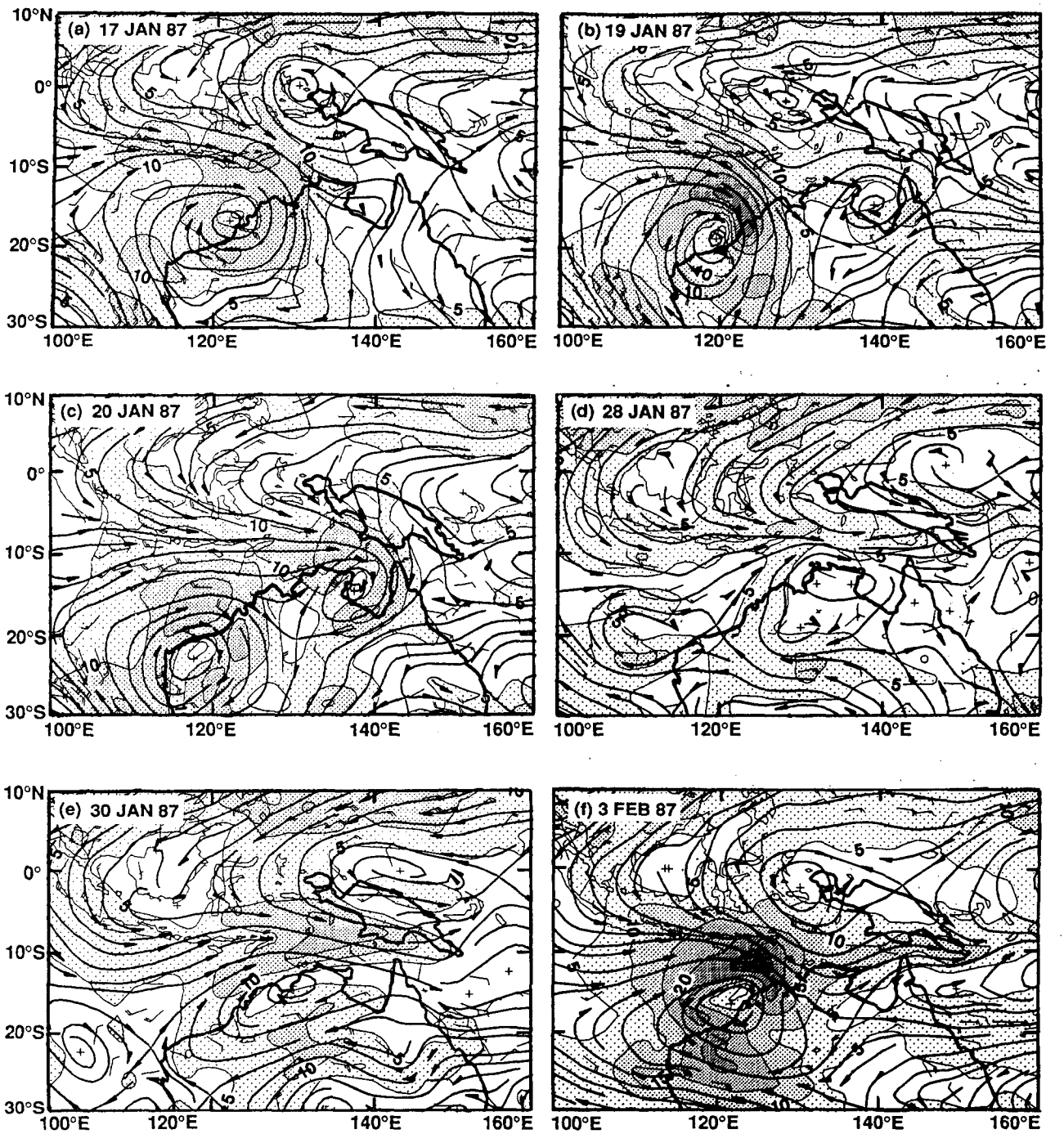

FIG. 10. Flow at the 850-hPa level for selected days. All maps are for 0000 UTC. Streamlines and isotachs (10 m s^{-1} intervals) are shown. Coastlines of Australia and the island of New Guinea are darkened. Adapted from Heckley and Puri (1988).

very similar pattern to the first. Once again, its formation corresponded to the beginning of the strengthening of the westerlies leading up to the second active period A2. This vortex also moved slowly westward (Fig. 10d), finally becoming stalled at a position near the western end of New Guinea (Fig. 10f). EMEX6 was flown at the time of Fig. 10d over the Joseph Bonaparte Gulf within the new Australian Low.

At the same time that the second New Guinea Vortex was moving westward, the new Australian Low was also moving westward, toward the west coast of Australia. EMEX7 was flown over the Joseph Bonaparte Gulf near the center of the Australian Low at the time

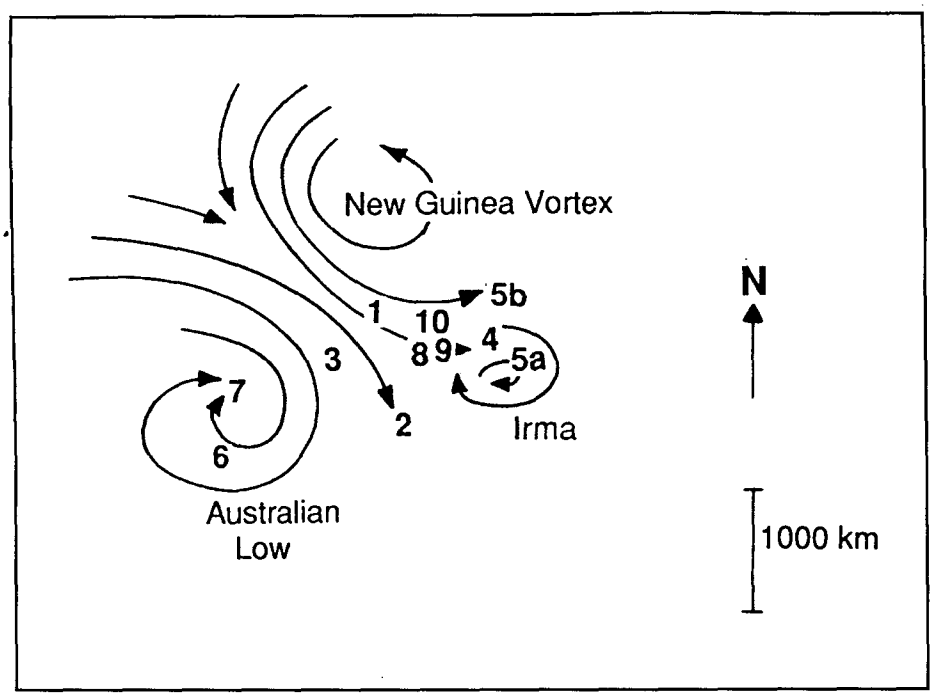

FIG. 11. Schematic map of the typical flow pattern at 850 hPa during EMEX and locations of the EMEX aircraft missions 1–10 (see Table 1) with respect to the circulation pattern. Mission EMEX5 has been subdivided into 5a and 5b.

of Fig. 10e. Later, when the center of the Australian Low was farther to the southwest (Fig. 10f), a tropical cyclone called Damian formed within the Australian Low. Eventually, Damian moved westward over the Indian Ocean, separating itself from the Australian Low, which remained near the west coast of Australia.

By 3 February, the middle of the A2 period, the vortex pair constituted by the New Guinea Vortex and Australian Low formed the pattern seen in Fig. 10f, which was very similar to that prevailing during the early part of active 1 (cf. Fig. 10a). At this time, Damian coincided with the center of the Australian Low. The aircraft missions EMEX8, 9, and 10 were all flown while the flow pattern resembled that in Fig. 10f. EMEX9 was being executed at exactly the time of this map. All three missions were carried out over the Arafura Sea, in the region of monsoonal westerlies located between the two vortices. These two vortices dominated the synoptic-scale flow pattern through 4 February, when the last mission (EMEX10) was conducted.

The New Guinea Vortex disappeared one day later on 5 February. On 7 February, another tropical cyclone (named Jason) formed over the Gulf of Carpentaria. Consequently, the last two days of active 2 resembled the last part of active 1, with the Australian Low and Jason constituting a map similar to that of Fig. 10c, which was dominated by the first Australian Low and Irma.

d. Summary of flights in relation to the large-scale circulation and the mean cloud patterns

The relationship of the EMEX aircraft missions to the synoptic-scale flow features described above is summarized schematically in Fig. 11, where the locations of all of the flights (plotted geographically in Fig. 3) have been transposed into a schematic map of the flow pattern at 850 mb, which prevailed during the active parts of the experiment.

The aircraft missions EMEX1, 2, 3, 5b, 8, 9, and 10 were all carried out in the downstream, diffluent region of the westerlies located between the New Guinea Vortex and Australian Low. EMEX2 was the farthest downstream, in the col at the very end of the region of westerlies. The cloud cluster sampled in this case was the smallest and exhibited the least amount of stratiform precipitation, although it contained a well-defined convective line. All the other EMEX missions within this group were flown well within the moist westerlies, where large cloud clusters were forming and undergoing their life cycles.

EMEX4 and 5a were flown in Irma. The majority of EMEX4 was focused on an outer rain band, which was investigated according to the EMEX flight plan indicated in Figs. 3 and 4. The early parts of EMEX4 and EMEX5a reconnoitered the structure of the hurricane center. EMEX6 and 7 were flown within the vicinity of the second Australian Low before the formation of Tropical Cyclone Damian.

The overall coverage of EMEX flights indicated by Fig. 11 suggests a concentration in the southern part of the monsoonal flow pattern and a near absence in the northern part. This apparent bias was partly a result of the fact that the AMEX network and the PRC ship lay in the southern part of the region. However, the mean satellite-observed cloud pattern (Fig. 9b), compared with the mean 850-mb flow (Fig. 9a), shows that the cloud systems in the EMEX region were, in fact, concentrated toward the downstream end of the monsoonal westerlies over the seas just north of the Australian

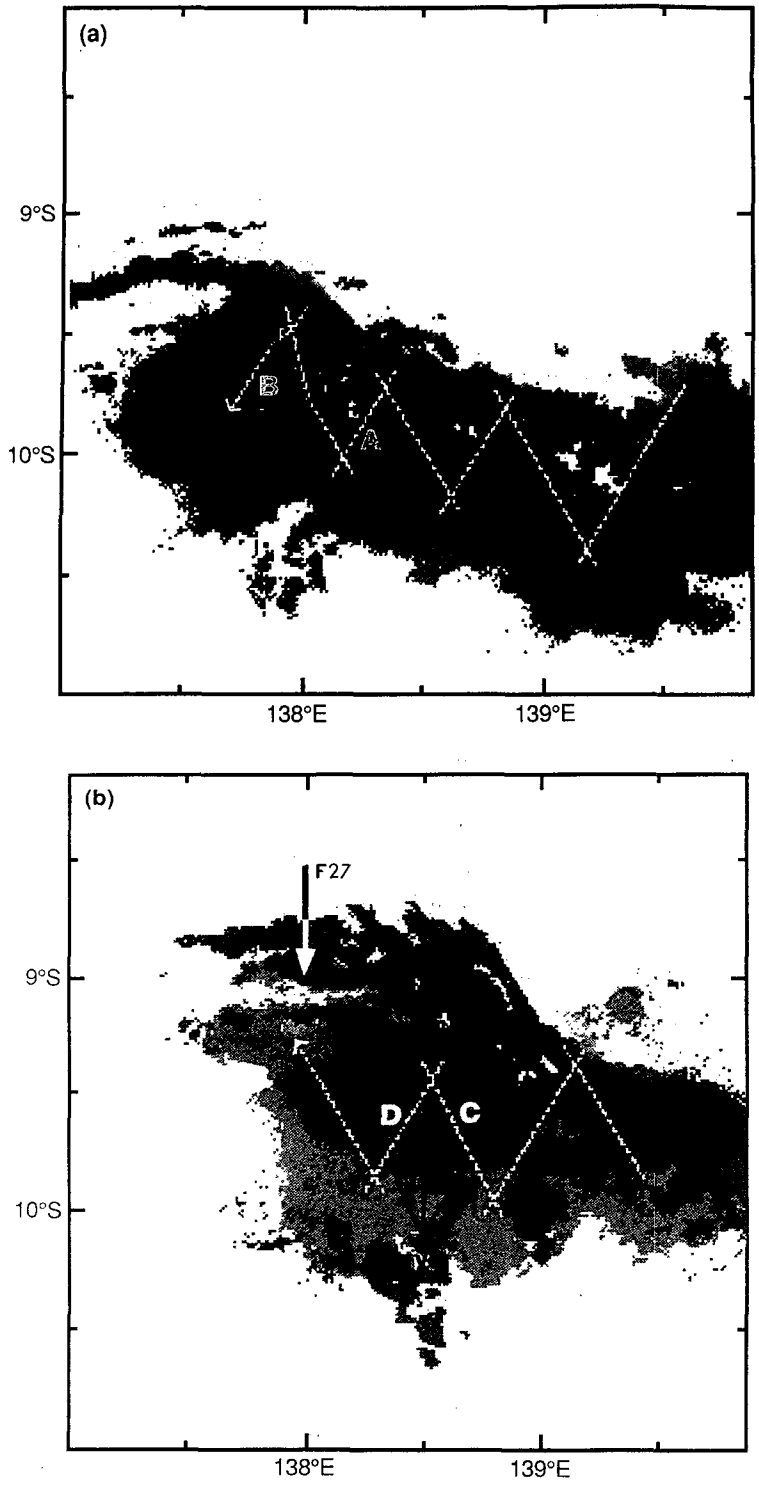

FIG. 12. (a) Time composite of radar reflectivity (dBZ) from the lower-fuselage radar aboard the P3 over the time interval 2040–2201 UTC 2 February 1987. Flight track of the P3 (westbound, as indicated by arrowhead on westernmost end) is shown in white. A and B are flight segments referred to in text. (b) As in (a), but for 2302–2350 UTC. C and D are flight segments referred to in text. A portion of the F27 flight track is also shown. The diamond-shaped region is the area for which divergence was calculated from the Doppler wind components perpendicular to the flight legs C and D. The line X–Y is the location of the cross section in Fig. 13.

land mass, which is where all flights took place (Fig. 2).

5. Examples of data collected during EMEX aircraft missions

In the following paragraphs we will briefly discuss some examples of the data collected during the flight program.

a. Aircraft mission EMEX9: 2 February 1987

To illustrate some of the types of data obtained in the EMEX flight program, we use mission EMEX9, which was flown over the Arafura Sea (Fig. 2) in the downstream, diffluent region of the westerlies located between the New Guinea Vortex and Australian Low (Fig. 11). The data obtained in this case have many similarities to those obtained in the other EMEX flights.

During the earlier part of the mission, the convective-transition part of the flight plan was executed in relation to a west-northwest to east-southeast oriented line of moderately intense convective precipitation observed with the lower-fuselage radar on the P3 aircraft (Fig. 12a)[8] Close inspection of this figure indicates that the westernmost portion of this convective band is characterized by a narrow line arcing northward. This arc-shaped feature intersected the remaining, straighter, east-southeastward-extending portion of

[8] The charts in Fig. 10 are composite radar echo maps compiled from the radar reflectivity measurements obtained with the P3 lower- fuselage radar during the indicated time period. All the recorded radar beams were transposed into a Cartesian geographical grid. Wherever grid elements were sampled by more than one sweep of the antenna, the value assigned to a given grid element was the maximum reflectivity value obtained on any of the sweeps. The use of the maximum is justified, since the recorded reflectivity from a single sweep is itself an average over many pulses and hence is a stable value. However, the value on a given sweep can be underestimated as a result of attenuation or other factors associated with the radar's characteristics or the geometry of the beam. It is difficult, however, to overestimate the value on a given sweep (unless the calibration of the radar is off). Hence, the best estimate of the true reflectivity at any geographical point is considered to be the maximum obtained on any given sweep.

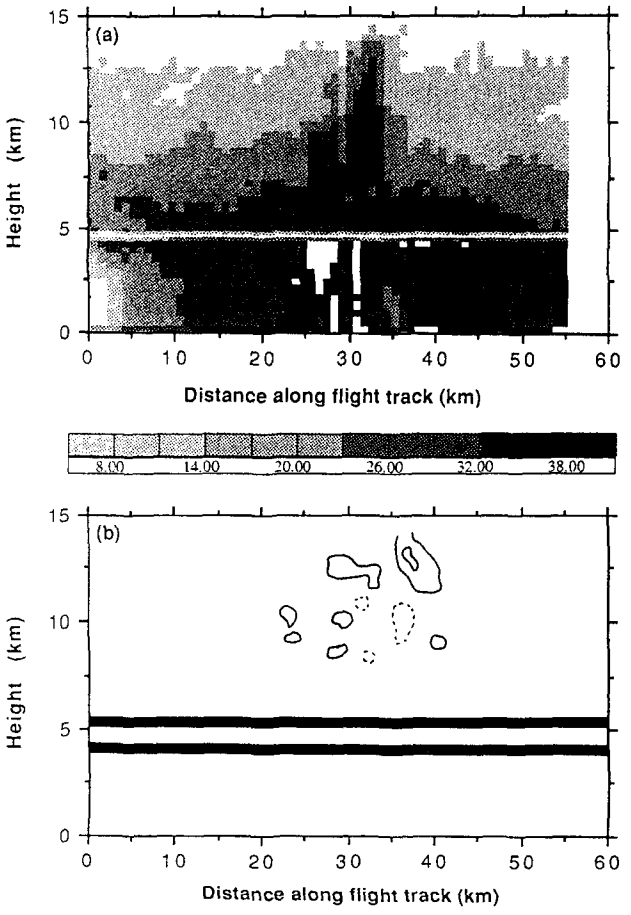

FIG. 13. Time–height section of vertically pointing data from the P3 tail radar for leg A in Fig. 9a. Time is converted to horizontal distance under the assumption of a ground speed of 140 m s^{-1}. (a) Radar reflectivity (dBZ) and (b) Doppler vertical velocity of the precipitation particles (m s^{-1}: solid contours +1, +3; dashed contour –4). Contours are shown only above the altitude of 0°C (EJ5km). Flight level (4.8 km) is evident in both panels. The Doppler range delay zones above and below the aircraft are contained within the heavy horizontal lines in (b).

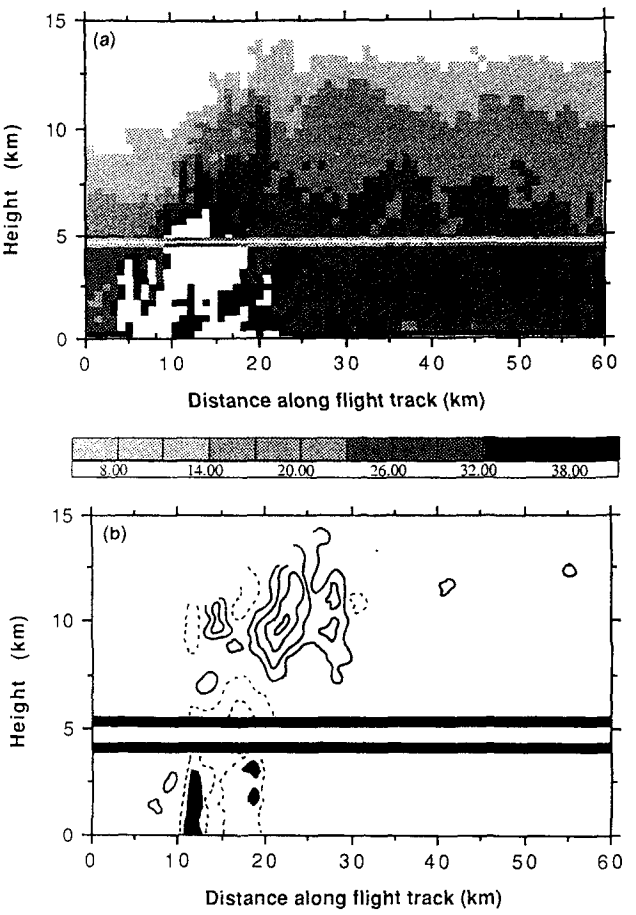

FIG. 14. Time–height section of vertically pointing data from the P3 tail radar for leg B in Fig. 12a. Time is converted to horizontal distance under the assumption of a ground speed of 140 m s^{-1}. (a) Radar reflectivity (dBZ) and (b) Doppler vertical velocity of the precipitation particles [m s^{-1}: solid contours +1, +3, +5, and +7; dashed contour –4 (above melting level only), –10; filled areas < –12 m s^{-1}]. Contours are shown only above the altitude of 0°C (EJ5km). Flight level (4.8 km) is evident in both panels. The Doppler range delay zone above and below the aircraft are contained within the heavy horizontal lines in (b).

the line at about 9.7°S, 138.0°E. Lighter, more uniform, stratiform precipitation is seen in the echo pattern both north and south of the convective line, with the largest stratiform region to the south and west of the intersection point.

The arc-shaped portion of the convective line moved rapidly (18 m s^{-1}) eastward during the hours after the time of Fig. 12a. By the time of Fig. 12b, the intersection point, marked by the most intense convective echo, lay at about 9.4°S, 138.9°E. The area of enhanced convection remained at the intersection point as long as this point was within range of the radar. The stratiform precipitation was generally present over a large area everywhere to the south of the convective line. It was especially strong southwest of the intersection point. In this region, the intense convection present at the intersection point earlier had undergone a transformation to form this strong stratiform precipitation. We observed such transitions of convective radar echo to strong stratiform echo frequently during the EMEX flights. The stratiform structure, characterized by a radar "bright band,"[9] was confirmed by data from the vertically scanning tail radar.

[9] As explained by Battan (1973), the radar bright band is a horizontal band of high reflectivity located in a 100–500-m-deep layer at an altitude just below the 0°C level and is associated with melting precipitation particles. It is considered to be the primary radar signature of stratiform precipitation, in which snow particles over a broad region are generally drifting downward because the vertical air motions in nimbostratus are considerably less than the fall velocity of the snow (1–2 m s^{-1}). Upon passing through the 0°C level, the particles melt and produce the bright band, whose horizontal character contrasts sharply with the vertical echo cores of cumulonimbus.

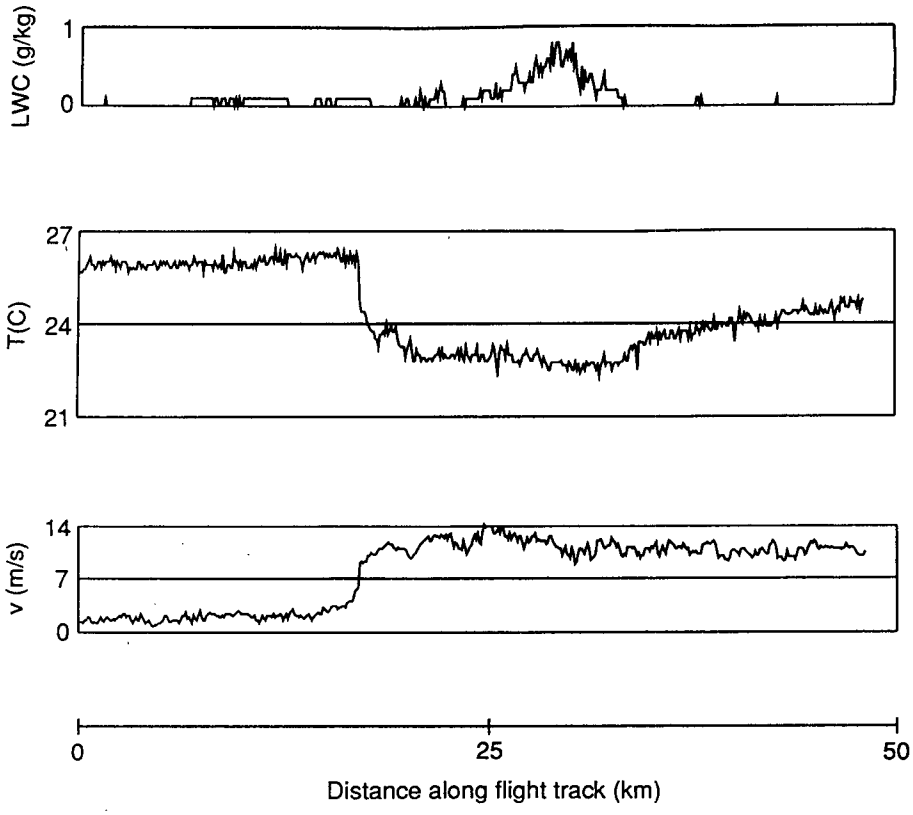

FIG. 15. Time-series of cloud liquid water content, temperature, and meridional wind v from the southbound flight leg of the F27.

In Fig. 12a, two flight-track segments transecting different parts of the precipitation area are indicated as segments A and B. Segment A cuts across a representative region of the convection east of the intersection point. Segment B crosses the arc-line near the intersection point. Time-height cross sections of data obtained with the tail radar while the P3 was flying along these segments are shown in Figs. 13 and 14. Comparison of the reflectivity patterns in Figs. 15 and 16 indicates that the convection east of the intersection point had an upright vertical structure and extended to a maximum height of about 14.5 km, while the convection in the arc line extended to a similar height but exhibited a pronounced rearward slope—a structure characteristic of tropical squall-line radar echoes (e.g., Houze 1977; Roux et al. 1984).

The vertical velocity of precipitation particles detected with the radar at vertical incidence along the two flight segments is shown in Figs. 13b and 14b. No attempt has been made to correct these motions for particle fallspeeds. Air motions can, however, be estimated for altitudes above the 0°C level (about 5 km above the ocean, which was, coincidentally, the approximate flight altitude) by adding about 1–2 m s^{-1} to the radar-detected velocities to account for the fallspeeds of the snow particles. For altitudes below 5 km, the air motions are obtained by adding 5–8 m s^{-1} to account for the fallspeeds of raindrops. With these corrections in mind, we see that the convection east of the intersection point was characterized by relatively weak, discrete bubbles of upward and downward motion, most evident at upper levels (Fig. 13b). The upper-level downdrafts appear to be similar to those seen in midlatitude mesoscale convective systems (Heymsfield and Schotz 1985; Smull and Houze 1987). The convection in the arc line was characterized by a stronger, rearward-sloping updraft as well as some convective-scale downdrafts aloft (Fig. 13b). The rearward-sloping updraft in the latter case is typical, characteristic of a tropical squall line whose reflectivity cell slopes like that in Fig. 13a (e.g., Roux et al. 1984). This rearward-sloping structure is also seen in many midlatitude squall lines (Houze et al. 1989).

The squall structure of the arc line was also demonstrated by low-level flight data from the F27 aircraft. Figure 15 shows time series of liquid water, temperature, and meridional wind from the southbound F27 flight leg indicated in Fig. 12b. These data were taken at the 990-mb level (about 100 m above the sea surface). At the cold pool edge, the F27 encountered sharp convergence and a 3°C temperature drop. The largest liquid water readings were recorded at about 5 km behind this gust front. The sudden wind and thermodynamic variations across the arc line seen in Fig. 15 strongly resemble those seen in other tropical squall lines (e.g., Houze 1977; Roux et al. 1984).

The P3 flight legs labeled C and D in Fig. 12b were flown in a region of stratiform precipitation. The radar echo in this region is seen to have been characterized by a well-defined bright band near the flight level at 4–4.5 km (Fig. 16). The Doppler-radar-detected horizontal wind components normal to flight legs C and D have been used to evaluate the line integral of the wind normal to the parallelogram drawn in Fig. 12b, between legs C and D. By Gauss's theorem, this line integral is equal to the mean horizontal divergence in this region. The vertical profile of divergence deter-

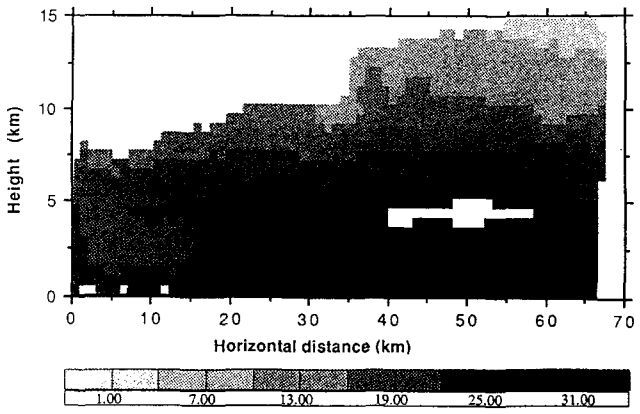

FIG. 16. Vertical cross section of radar reflectivity (dBZ) along segment X–Y in Fig. 12b. On the distance scale, 0 corresponds to point Y and 70 to point X.

mined by this technique is shown in Fig. 17. The profile shows divergence in the lower and upper troposphere and convergence in the middle troposphere. Such a profile is characteristic of the divergence in the stratiform regions of mesoscale convective systems (Houze 1989).

b. Radiation profiles during EMEX8

Radiation profiles were conducted by the P3 on each of the EMEX missions along the patterns shown in Fig. 4c. The principal aim was to test the Webster–Stephens hypothesis regarding the radiative destabilization of the stratiform region. EMEX9 offered an unprecedented opportunity to obtain not only a radiation profile from the P3 in and below the anvil, but also data from above the anvil from the ER2 operating at 16 km and in the

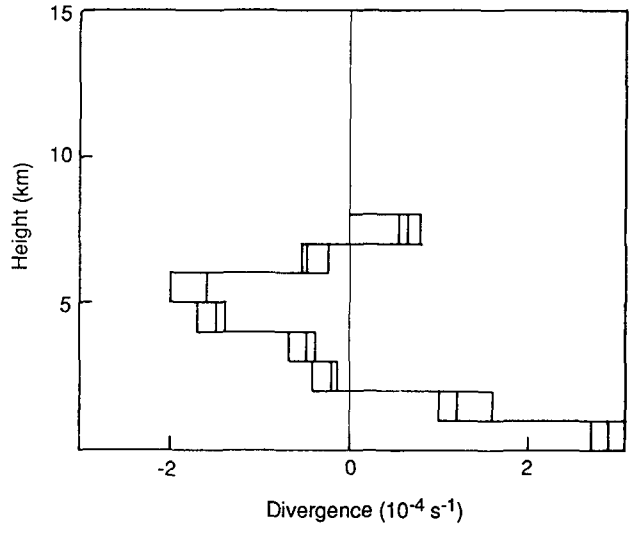

FIG. 17. Vertical profile of average divergence within the parallelogram indicated in Fig. 12b. The three profiles are independent estimates constructed by shifting the parallelogram by 1 radar-range interval.

boundary layer from the F27. Figure 18 shows the radiation measurements averaged over each leg and normalized according to the mean time of each leg of the P3. The radiation profile was taken between 0026z and 0117z (i.e., 0926 and 1007 local) on flights along 9.4°S, back and forth across 139°E, 1–2 h after the time of Fig. 12b. The stratiform cloud top and bottom were located at 15 and 4.5 km, respectively. No data existed between 7 km, the initial flight level of the P3, and 16 km. In these regions, a simple linear interpolation was employed. In the same manner, a similar extrapolation was used to extend the profiles from the F27 flight level to the ocean surface. The upward shortwave radiation was not included in the calculations because of instrument problems.

Figure 18 shows that the large optical thickness of the stratiform cloud is manifested by an 85% extinction of the solar beam. Little attenuation of the upward and downward solar beam below the anvil is shown by the parallel nature of the two beams, suggesting very little solar heating. The upward and downward infrared radiation show similar features to the solar radiation. Individually, each infrared stream indicates radiational convergence below the cloud. However, the two streams offset each other, thus reducing the net infrared heating. However, the values of each stream are so large (order 400–500 w m^{-2}) that even a small difference in the slope of the profiles could indicate substantial heating. The main point of the figure is that there is relatively little radiative heating at or below the cloud base, while at the cloud top there is both solar heating and infrared cooling. The data are consistent in general with the calculations of Webster and Stephens (1980) and Churchill and Houze (1991). The latter show, by model calculations, that the solar heating penetrates more deeply into the cloud layer than does the radiative cooling. Destabilization associated with the net cooling is confined to the top 1 km or so of the cloud. More studies combining modeling and the EMEX radiation profiles are to be carried out (e.g., Wong et al. 1990).

6. Conclusions and outlook for future research

The overview of EMEX and the examples of data obtained in the experiment presented above indicate the successful documentation of the kinematic structure of a representative sample of near-equatorial oceanic cloud clusters. Ten aircraft missions resulted in ten successful penetrations of cloud clusters. In each case, several hours of data were collected according to a systematic sampling scheme. Roughly equal amounts of data were obtained in convective

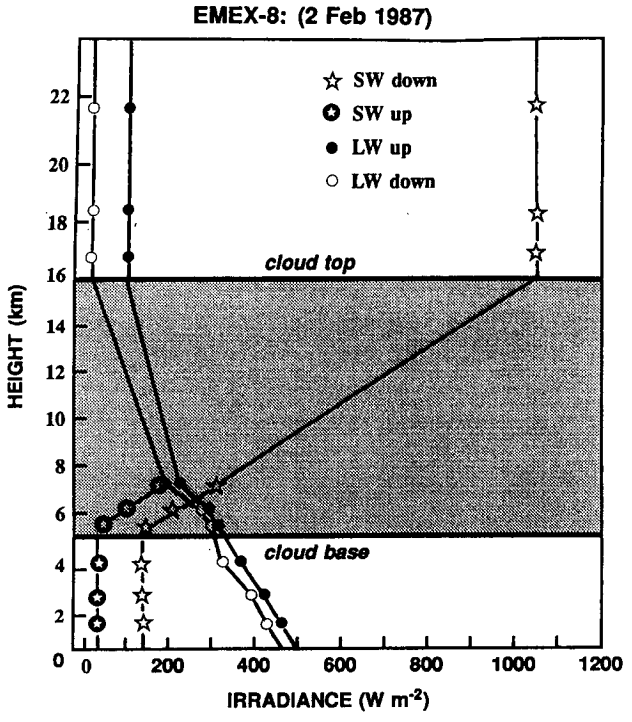

FIG. 18. Normalized EMEX8 radiation measurements from the NOAA P3, the NASA ER2, and the CSIRO F27. From Wong et al. 1990.

precipitation, stratiform precipitation and precipitation that was in transition from convective to stratiform structure.

The EMEX data is available for the use by interested investigators. A list of the data and contact points is given in appendix B. Contact points for the ancillary experiments (STEP and AMEX) are also listed.

Because the data were collected in a series of V-shaped flight legs, dual-Doppler analysis techniques can be applied to determine the vertical profile of divergence in the convective, stratiform, and transitional areas. In all, 111 V-shaped pairs of flight legs are available to analyze. The example of a stratiform-region profile shown in this paper is similar to the stratiform-region divergence profiles seen in the stratiform regions of other tropical cloud clusters. Current work indicates that the divergence profiles in convective and transitional regions can also be determined (Mapes and Houze 1990, 1991). An important result of EMEX will then be a determination of the average vertical profiles of divergence in convective, transitional, and stratiform regions in a reasonably large sample of oceanic cloud clusters. Integration of these vertical profiles will yield the vertical distribution of vertical velocity in these regions. It will then be possible to estimate the vertical distribution of heating in the clusters and to see the contributions to this distribution by the convective, transitional, and stratiform components of the cloud clusters. This was the primary objective of EMEX.

The vertical-incidence Doppler radar observations add further insight into the nature of the convective motions. They reveal details that cannot be seen in the mean profiles of divergence and vertical velocity. They also reveal details of the updraft and downdraft core structures that could not be seen in the earlier Zipser–LeMone studies, which were based on flight-level data. There were two distinct structures among the cells in the convective regions of the cloud system. The convective cells exhibited strong slope in the arc-shaped squall-line component of the convective band, while in the remainder of the band the cells had a more upright structure. The vertical incidence data further allows the vertical motion structure at high levels to be deduced. From these data, it appears that the strongest updrafts are at very high levels and that upper-level downdrafts are a common feature of the convective regions in tropical cloud clusters.

Data from the Electra, F27, and the ER2 aircraft flights conducted in coordination with the P3 also add detail and insight to the airborne Doppler data collected aboard the P3. We have seen an example of how the F27 confirms the squall character of the arc line observed during EMEX9. The vertical velocities, horizontal winds, and thermodynamic data collected in the lower troposphere by the Electra and F27 can be used in many other situations to check the consistency of the Doppler radar observations and to add to the general understanding of each individual cloud cluster investigated. We have also seen how radiation data collected by the ER2, P3, and the F27 can be combined to give an estimate of the in-cloud radiative heating profile in the stratiform region of a mesoscale convective system.

EMEX may be considered to be the first atmospheric process study of TOGA. The data collected is central to an understanding of the large-scale processes that drive the tropical systems. Information gained in EMEX has helped guide the development of the TOGA Coupled Ocean–Atmosphere Response Experiment (TOGA COARE). The principal aims of COARE build upon those of EMEX by seeking the processes that mutually drive the ocean and the atmosphere in the warm-pool regions of the western Pacific Ocean.

Acknowledgments. EMEX could not have been carried out without the aircraft facilities provided by NOAA and NCAR of the United States, and CSIRO of Australia, the ship provided by the People's Republic of China, and the ground support of the Australian Bureau of Meteorology and Royal Australian Air Force. In particular, we would like to thank Dr. J. Zillman, director of the Australian Bureau of Meteorology, and Dr. G. Love, regional director of the Bureau of

APPENDIX A: Principal investigators and affiliations

Investigator	Institution
R. A. Houze, Jr.	Department of Atmospheric Sciences, University of Washington
P. J. Webster	Department of Meteorology, The Pennsylvania State University
G. Barnes	The National Center for Atmospheric Research
R. Burpee	National Hurricane Research Division, NOAA
W. Frank	Department of Meteorology, The Pennsylvania State University
S. Geotis	Center for Meteorology and Physical Oceanography, Massachusetts Institute of Technology
F. D. Marks, Jr.	National Hurricane Research Division, NOAA
B. Ryan	Division of Atmospheric Research, CSIRO, Australia
G. L. Stephens	Department of Atmospheric Sciences, Colorado State University
M. Williams	Australian Bureau of Meteorology
G. Young	Department of Meteorology, The Pennsylvania State University
E. J. Zipser	The National Center for Atmospheric Research

Meteorology in the northern territory, who made available personnel and facilities and made EMEX possible. Furthermore, we would like to acknowledge the support of Dr. Chao Jiping, director of the PRC State Oceanographic Administration for his support of EMEX, in general, and for making the Xiang Yang Hong No. 5 available. We would like to acknowledge our AMEX colleagues, Drs. Holland, Keenan, and McBride, without whose efforts EMEX would have been a lesser experiment. Finally, we owe a special appreciation to the U.S. TOGA Office, and its director, Dr. M. Hall, who, together with Dr. J. Theon of NASA, made possible the construction of the TOGA Doppler radar through considerable effort. The P3 aircraft operation was directed by Drs. R. Burpee and F. Marks and Captain T. Gerrish of NOAA, the Electra by Dr. G. Barnes of NCAR, and the F27 by Dr. B. Ryan of CSIRO. Forecasting for the flight operations was done by Mr. M. Williams of the Australian Bureau of Meteorology. Special thanks are due to Ms. Tracey Smail and Ms. Karyn Sawyer-Crouch who, together with Mr. Gene Martin, oversaw the logistics of the experiment and its successful meshing with the other two concurrent research endeavors.

We would like to dedicate this paper to our Chinese colleagues who, with Speed Geotis, of MIT, stayed on station aboard the Xiang Yang Hong No. 5 in the Gulf of Carpentaria through hurricane-force winds, and to the crews and engineers of the EMEX aircraft.

The authors' individual research was supported by the National Science Foundation under Grants ATM-8617118 and ATM-8616647A02 and the Office of Naval Research University Research Initiative N00014-86-K-0688. Computing facilities were made available by NCAR and data by the European Centre for Medium Weather-Range Forecasts.

References

Battan, L. J., 1973: *Radar Observation of the Atmosphere.* University of Chicago Press, 324 pp.

Chang, H.-R., and P. J. Webster, 1990: Energy accumulation and emanation at low latitudes. Part II: Nonlinear response to strong episodic equatorial forcing. *J. Atmos Sci.,* **47,** 2624–2644.

Charney, J. C., 1969: A further note on large-scale motions in the tropics. *J. Atmos Sci.,* **26,** 607–609.

Churchill, D., and R. A. Houze, Jr., 1991; Effects of radiation and turbulence on the diabatic heating and water budget of the stratiform region of a tropical cloud cluster, *J. Atmos Sci.,* **48,** 903–922.

Gamache, J. F., and R. A. Houze, Jr., 1982: Mesoscale air motions associated with a tropical squall line. *Mon. Wea. Rev.,* **110,** 118–135.

——, and ——, 1985: Further analysis of the composite wind and thermodynamic structure of the 12 September GATE squall line. *Mon. Wea. Rev.,* **113,** 1241–1259.

——, F. D. Marks, Jr. and R. W. Burpee, 1987: EMEX data report: The Equatorial Mesoscale Experiment. AOML/HRD Report, National Oceanic and Atmospheric Administration, Atlantic Oceanographic and Meteorological Laboratory.

Hartmann, D. L., H. H. Hendon, and R. A. Houze, Jr., 1984: Some implications of the mesoscale circulations in tropical cloud clusters for large-scale dynamics and climate. *J. Atmos. Sci.,* **41,** 113–121.

Heckley, W. A., and K. Puri, 1988: The winter monsoon during AMEX: A quick look atlas. Report, European Centre for Medium-Range Forecasts, 10 pp. [Available from the European Centre for Medium–Range Weather Forecasts, Shinfield Park, Reading, Berkshire, RG2 9AX, United Kingdom.]

Heymsfield, G. M., and S. Schotz, 1985: Structure and evolution of a severe squall line over Oklahoma. *Mon. Wea. Rev.,* **113,** 1563–1589.

Holland, G. J., J. L. McBride, R. K. Smith, D. Jasper and T. D. Keenan, 1986: The BMRC Australian Monsoon Experiment: AMEX. *Bull. Amer. Meteor. Soc.,* **67,** 1466–1472.

Houze, R. A., Jr., 1977: Structure and dynamics of a tropical squall-line system. *Mon. Wea. Rev.,* **105,** 1540–1567.

——, 1982: Cloud clusters and large-scale vertical motions in the tropics. *J. Meteor. Soc. Japan,* **60,** 396–410.

——, 1989: Observed structure of mesoscale convective systems and implications for large-scale heating. *Quart. J. Roy. Meteor. Soc.,* **115,** 425-461.

——, and E. N. Rappaport, 1984: Air motions and precipitation structure of an early summer squall line over the eastern tropical Atlantic. *J. Atmos. Sci.,* **41,** 553–574.

——, S. J. Bograd, and B. Mapes, 1988: An atlas of horizontal patterns of radar reflectivity observed during EMEX aircraft missions. Report, Department of Atmospheric Sciences, University of Washington, 142 pp.

——, S. A. Rutledge, M. I. Biggerstaff, and B. F. Smull, 1989: Interpretation of Doppler weather-radar displays of midlatitude mesoscale convective systems. *Bull. Amer. Meteor. Soc.,* **70,** 608–619.

APPENDIX B: Contact points for experiment data

	Data	Contact	Address
1. EMEX			
• NCAR Electra	Flight-level and ODW data	Dr. G. Barnes	National Center for Atmospheric Research P.O. Box 3000, Boulder, CO 80307
• CSIRO F27	Flight-level data	Dr. B. Ryan	Division of Atmospheric Research, Private Bag #1, Mordialloc, Victoria, Australia
• NOAA WD-P3	Radar and particle measuring systems data	Prof. R. Houze, Jr.,	Dept. of Atmospheric Sciences, University of Washington, AK-40, Seattle, WA 98195
• NOAA WD-P3	Flight-level and ODW data	Dr. J. Gamache	NOAA/AOML Hurricane Research Division, 4301 Rickenbacker Causeway, Miami, FL 33149, USA
• NOAA WD-P3 Electra, F27	Radiation-flux data	Dr. G. L. Stephens	Department of Atmospheric Science, Colorado State University, Fort Collins, CO 80532, USA
• Xiang Yang Hong No. 5	Doppler radar	Dr. S. Geotis	Weather Radar Research Group, Center for Atmospheric Science and Physical Meteorology, Building 54/1815, Massachusetts Institute of Technology, Cambridge MA 02139
2. AMEX		Dr. G. Holland	Bureau of Meteorology Research Centre, P.O. Box 1289K, GPO, Melbourne, Vic., 3001, Australia
3. STEP		Dr. L. Pfister	NASA AMES, Moffett Field, CA 94035

Johnson, R. H., 1976: The role of convective-scale precipitation downdrafts in cumulus and synoptic-scale interactions, *J. Atmos. Sci.,* **42,** 1890–1910.

Jorgensen, D. P., E. J. Zipser, and M. A. LeMone, 1985: Vertical motions in intense hurricanes. *J. Atmos. Sci.,* **42,** 839–856.

Keenan, T. D., and S. C. Martin, 1987: AMEX Radar Atlas, Volume II: AMEX Phase II. BMRC Research Report No. 9, Bureau of Meteorology Research Centre, 147 pp. [Available from the Bureau of Meteorological Research Centre, GPO Box 1289K, Melbourne, Vic 3001, Australia.]

Kuettner, J. P., and D. E. Parker, 1976: GATE: Report on the field phase. *Bull. Amer. Meteor. Soc.,* **57,** 11–27.

Lau, K.-M., L. Peng, C. H. Sui and T. Nakazawa, 1989: Dynamics of supercloud clusters, westerly wind bursts, 30–60 day oscillations and ENSO: A unified view. *J. Meteor. Soc. Japan,* **67,** 205–219.

LeMone, M. A., 1983: Momentum transport by a line of cumulonimbus. *J. Atmos. Sci.,* **40,** 1815–1834.

——, and E. J. Zipser, 1980: Cumulonimbus vertical velocity events in GATE. Part I: Diameter, intensity, and mass flux. *J. Atmos. Sci.,* **37,** 2444–2457.

Mapes, B., and R. A. Houze, Jr., 1990: Divergence profiles in tropical mesoscale convective systems. *Extended Abstracts, Fourth Conf. on Mesoscale Processes,* Boulder, Amer. Meteor. Soc., 202–203.

——, and ——, 1991: An integrated view of the Australian monsoon and its mesoscale convective systems. Part 1: Horizontal structures. *Quart. J. Roy. Meteor. Soc.* (submitted).

Marks, F. D., Jr. 1986: EMEX Research Aircraft Plan. AOML/HRD Report, National Oceanic and Atmospheric Administration, Atlantic Oceanographic and Meteorological Laboratory, Miami, 15 pp..

Ramage, C. S., 1968: Role of a tropical "maritime continent" in the atmospheric circulation. *Mon. Wea. Rev.,* **96,** 365–370.

Reed, R. J., and E. E. Recker, 1971: Structure and properties of synoptic scale wave disturbances in the equatorial Pacific. *J. Atmos. Sci.,* **28,** 1117–1133.

Roux, F., J. Testud, M. Payen, and B. Pinty, 1984: West African squall-line thermodynamic structure retrieved from dual-Doppler radar observations. *J. Atmos. Sci.,* **41,** 3104–3121.

Sommeria, G., and J. Testud, 1984: COPT81: A field experiment designed for the study of dynamics and electrical activity of deep convection in continental tropical regions. *Bull. Amer. Meteor. Soc.,* **65,** 4–10.

Smull, B. F., and R. A. Houze, Jr., 1987: Dual-Doppler radar analysis of a midlatitude squall line with a trailing region of stratiform rain. *J. Atmos. Sci.,* **44,** 2128–2148.

Thompson, R. M., Jr., S. W. Payne, E. E. Recker, and R. J. Reed, 1979: Structure of synoptic-scale wave disturbances in the intertropical convergence zone of the eastern Atlantic Ocean, *J. Atmos. Sci.,* **36,** 53–71.

Warner, C., and D. P. McNamara, 1984: Aircraft measurements of convective draft cores in MONEX. *J. Atmos. Sci.,* **41,** 430–438.

Webster, P. J., 1983: The large scale structure of the tropical

atmosphere. *Large Scale Dynamical Processes in the Atmosphere,* B. Hoskins and R. Pearce, Eds., Academic Press, 235–276.
——, 1987: The elementary monsoon. *Monsoons,* J. S. Fein and P. L. Stephens, Eds., J. Wiley and Sons, 3–32.
——, and G. L. Stephens, 1980: Tropical upper-tropospheric extended clouds: Inferences from Winter MONEX. *J. Atmos. Sci.,* **37,** 1521–1541.
——, and H-.R. Chang, 1988: Equatorial energy accumulation and emanation regions: Impact of a zonally varying basic state. *J. Atmos. Sci.,* **45,** 803–829.
Williams, M., and R. A. Houze, Jr., 1987: Satellite-observed characteristics of winter monsoon cloud clusters. *Mon. Wea. Rev.,* **115,** 505–519.
Wong, T., P. Stackhouse, G. Stephens, and F. Valero, 1990: A comparison of cloud radiation fields obtained by in situ aircraft measurements and a numerical simulation of a tropical mesoscale convective system, *Proc. American Meteorological Society Radiation Conference,* San Francisco, Amer. Meteor. Soc., 46–50.
World Climate Research Programme, 1990: Scientific Plan for the Coupled Ocean–Atmosphere Response Experiment, WCRP publication 64, Addendum 3, World Meteorological Organization, Geneva, Switzerland, 95 pp.
Yanai, M., S. Esbensen, and J. H. Chu, 1973: Determination of the bulk properties of tropical cloud clusters from large-scale heat and moisture budgets, *J. Atmos. Sci.,* **30,** 611–627.
Zipser, E. J., and M. A. LeMone, 1980: Cumulonimbus vertical velocity events in GATE. Part II: Synthesis and model core structure. *J. Atmos. Sci.,* **37,** 2458–2469.